Supplementary Information

Enhancement of photoinduced reactive oxygen species generation in open-cage fullerenes

Cristina Castanyer,[a,] † Çetin Çelik,[b,]† Albert Artigas,[a] Anna Roglans,[a] Anna Pla-Quintana,*[a] Antony Stasyuk, *[a,c,d] Yoko Yamakoshi,*[b] and Miquel Sola*[a]

[a] Institut de Quimica Computacional i Catàlisi (IQCC) and Departament de Química, Universitat de Girona, M. Aurèlia Capmany, 69, 17003 Girona, Catalonia, Spain. E-mail: anna.plaq@udg.edu; antony.stasuk@gmail.com; miquel.sola@udg.edu

[b] Department of Chemistry and Applied Biosciences, ETH Zürich, Vladimir-Prelog-Weg 3, CH-8093 Zürich, Switzerland. E-mail: yamakoshi@org.chem.ethz.ch

[c] Faculty of Chemistry, University of Warsaw, Pasteura 1, 02-093 Warsaw, Poland

[d] Departament de Farmàcia i Tecnologia Farmacèutica, i Fisicoquímica, Facultat de Farmàcia i Ciències de l'Alimentació & Institut de Química Teòrica i Computacional (IQTCUB), Av. Joan XXIII 27-31, Universitat de Barcelona (UB), Barcelona, Catalonia, Spain

TABLE OF CONTENTS

General information

Unless otherwise noted, materials were obtained from commercial suppliers and used without further purification. CH_2Cl_2 was dried under nitrogen by passing through solvent purification columns (MBraun, SPS-800). Reaction progress during the preparation of all compounds was monitored using thin layer chromatography on Macherey-Nagel Xtra SIL G/UV254 silica gel plates. Solvents were removed under reduced pressure with a rotary evaporator. Reaction mixtures were chromatographed on silica gel. All ^{1}H and ^{13}C NMR spectra were recorded on a Bruker ASCEND 400 spectrometer equipped with a 5 mm BBFO probe or and Bruker 600 spectrometre equipped with a CryoProbe (Bruker BioSpin GmbH, Rheinstetten, Germany) using $CDCl_3$ as a deuterated solvent. Chemical shifts for ^{1}H and ^{13}C NMR are reported in ppm (δ) relative to residual solvent signals. Coupling constants are given in Hertz (Hz). ^{1}H and ^{13}C NMR signals were assigned based on 2D-NMR HSQC, HMBC and COSY experiments when necessary. Mass spectrometry analyses were recorded on a Bruker micrOTOF-Q II mass spectrometer (high resolution), equipped with electrospray ion source and a Bruker Daltonics solariX spectrometer. The instruments were operated in the positive ESI (+) ion mode. IR spectra were recorded on an Agilent Cary 630 FT-IR spectrometer equipped with an ATR sampling accessory. UV-vis spectroscopy was performed on a Varian Cary-500 spectrophotometer with 1 cm quartz cells. Cyclic voltammetry was carried using a J-Cambria IH-660 potentiostat.

Synthesis of C_{60} derivatives 1-3

Scheme S1. Synthesis of compound **1**.

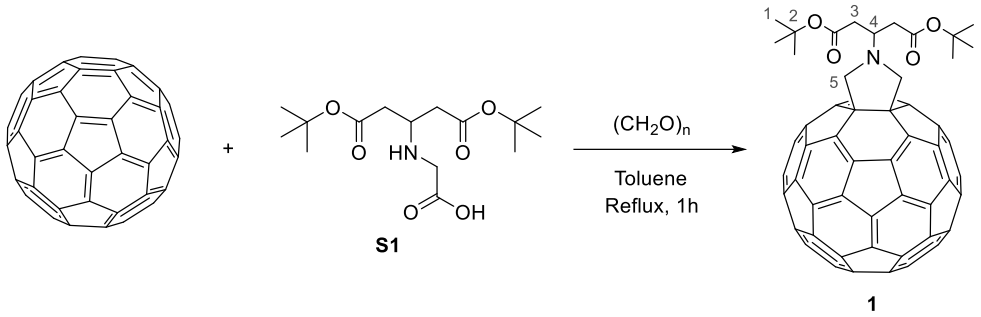

Compound 1. Compounds **S1** and **1** were prepared by reported methods.[1] A mixture of paraformaldehyde (15.0 mg, 0.50 mmol) and **S1** (69.7 mg, 0.22 mmol) was added to a solution of C_{60} (100.2 mg, 0.14 mmol) in toluene (90 mL) and the mixture was refluxed for 1 h. The product was purified by column chromatography on silica gel using toluene as the eluent. Unreacted C_{60} (24.3 mg) was first eluted and further elution afforded compound **1** (47.8 mg, 34%, 45% yield based on consumed C_{60}) as a dark solid. **MW** ($C_{75}H_{27}NO_4$): 1006.0; **Rf:** 0.3 (toluene); **^{1}H NMR ($CDCl_3$, 400 MHz) δ(ppm):** 1.57 (s, 18H, H1), 2.80 (dd, *J* = 15.0, 6.6 Hz, 2H, H3), 2.98 (dd, *J* = 15.0, 6.6 Hz, 2H, H3'), 4.21 (quint, *J* = 6.6 Hz, 1H, H4), 4.55 (s, 4H, H5); **^{13}C NMR ($CDCl_3$, 150 MHz) δ(ppm):** 28.4 (C1), 38.5 (C3), 54.8 (C4), 63.3 (C5), 69.9, 81.4 (C2), 136.6, 140.3, 142.0, 142.2, 142.3, 142.8, 143.2, 144.7, 145.4, 145.6, 145.9, 146.1, 146.2, 146.4, 147.5, 154.9, 171.1 (C=O); **ESI-HRMS (*m/z*)** calculated for $[M+H]^+$= 1006.2013; found 1006.2002.

Scheme S2. Synthesis of compound **2**.

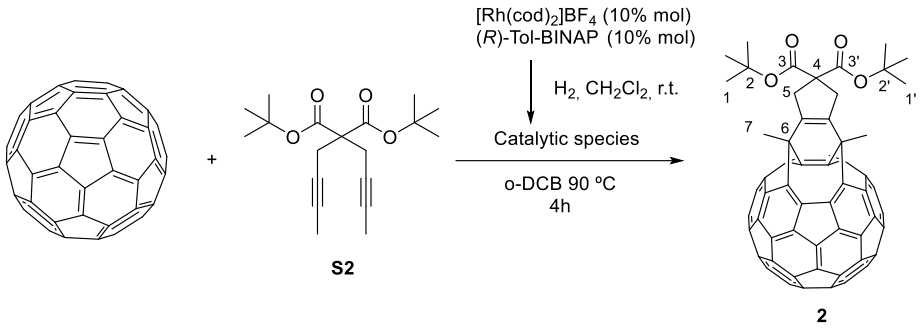

Compound 2. Compound **S2** was prepared by a reported method.[2] Compound **2** was prepared following the reported method:[3] A solution of $[Rh(cod)_2]BF_4$ (2.8 mg, 0.007 mmol) and (*R*)-Tol-BINAP (5.0 mg, 0.007 mmol) in anhydrous CH_2Cl_2 (4 mL) was prepared in a 10 ml capped vial in an inert atmosphere. Hydrogen gas was bubbled into the catalyst solution for 30 min before it was concentrated to dryness, dissolved in anhydrous *o*-dichlorobenzene and introduced into a solution of C_{60} (53 mg, 0.073 mmol) and **S2** (0.13g, 0.41 mmol) in anhydrous *o*-dichlorobenzene (1.4 mM) preheated at 90 °C. The resulting mixture was stirred at 90 °C for 4h. The crude reaction was purified by column chromatography on silica gel using CS_2 as the eluent. Unreacted C_{60} (24 mg) was first eluted and further elution with toluene/hexanes (1:1) afforded compound **2** (31.7 mg, 41%, 76% yield based on consumed C_{60}) as a dark solid. **MW** ($C_{79}H_{28}O_4$): 1041.1; **Rf:** 0.36 (toluene/hexanes 1:1); **IR (ATR) ν (cm^{-1}):** 2914, 1722; **^{1}H NMR (CDCl$_3$, 400 MHz) δ(ppm):** 1.49 (s, 9H, H1), 1.54 (m, 9H, H1'), 2.88 (s, 6H, H7), 3.21-3.27 (m, 2H, H5), 3.34-3.40 (m, 2H, H5'); **^{13}C NMR (CDCl$_3$, 101 MHz) δ(ppm):** 27.92 (C1), 27.95 (C1'), 28.1 (C7), 39.9 (C5), 44.4 (C6), 59.8 (C4), 81.7 (C2), 81.8 (C2'), 126.7, 135.2, 135.7, 136.5, 136.8, 137.1, 137.6, 139.0, 139.1, 140.0, 140.1, 140.5, 140.9, 143.3, 143.4, 143.6, 143.7, 143.8, 143.9, 144.0, 144.4, 144.5, 144.6, 144.7, 145.2, 145.3, 145.7, 145.8, 149.8, 151.8, 170.6 (C3), 170.9 (C3'); **UV-Vis (CHCl$_3$) λ (nm):** 264, 327; **ESI-HRMS (*m/z*)** calculated for $[M+Na]^+$= 1063.1880; found 1063.1877.

Scheme S3. Synthesis of compound **3**.

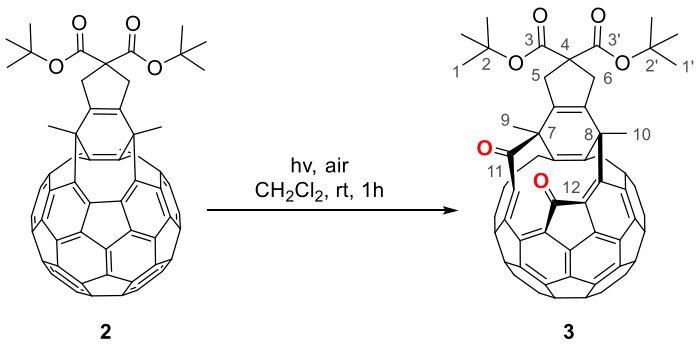

Compound 3. Compound **3** was prepared following the reported method:[3,4] A solution of **2** (20 mg, 0.02 mmol) in CH_2Cl_2 (14 mL) was exposed to light and air for 1 h. The crude reaction was purified by column chromatography on silica gel using CH_2Cl_2/hexanes (from 1:1 to 2:1) as the eluent, affording **3** (13.6 mg,

66%) as a dark solid. **MW** ($C_{79}H_{28}O_6$): 1073.1; **Rf:** 0.2 (hexanes/CH_2Cl_2 1:1); **IR (ATR) ν (cm^{-1}):** 2919, 1722; **^{1}H NMR ($CDCl_3$, 400 MHz) δ(ppm):** 1.60 (s, 9H, H1), 1.68 (s, 9H, H1'), 2.29 (s, 3H, H9), 2.63 (s, 3H, H10), 3.44 (d, *J* = 16.0 Hz, 1H, H5/H6), 3.72 (d, *J* = 16.8, 1H, H5/H6), 4.05 (d, *J* = 16.0 Hz, 1H, H5/H6), 4.34 (d, *J* = 16.8, 1H, H5/H6);**^{13}C NMR ($CDCl_3$, 101 MHz) δ(ppm):** 28.2 (C1), 28.3 (C1'), 32.0 (C9), 32.3 (C10), 40.3 (C5/C6), 41.6 (C5/C6), 43.6 (C8), 52.4 (C7), 60.3 (C4), 81.5 (C2+C2'), 129.3, 131.6, 131.8, 132.0, 132.3, 133.2, 133.3, 135.4, 135.8, 135.9, 136.2, 136.3, 136.7, 137.12, 137.13, 137.6, 137.8, 138.8, 139.7, 140.0, 140.3, 140.4, 140.5, 140.6, 140.9, 141.0, 141.3, 141.8, 142.0, 142.5, 142.8, 142.9, 143.0, 144.2, 144.4, 144.5, 144.73, 144.75, 145.24, 145.25, 145.5, 145.78, 145.80, 145.86, 145.91, 145.94, 146.0, 146.08, 146.13, 146.2, 146.4, 146.5, 147.1, 147.5, 147.8, 147.89, 147.93, 148.8, 150.0, 151.1, 155.9, 170.7 (C3), 172.3 (C3'), 191.4 (C12), 202.6 (C11); **UV-Vis ($CHCl_3$) λ (nm):** 256, 323; **ESI-HRMS (*m/z*)** calculated for $[M+Na]^+$= 1095.1778; found 1095.1768.

Absorption spectroscopic characterization of 1-3

UV-Vis spectroscopy for compounds **1**-**3** was performed on a Cary 50 Scan (Varian) UV-Vis spectrophotometer with 1 cm quartz cells.

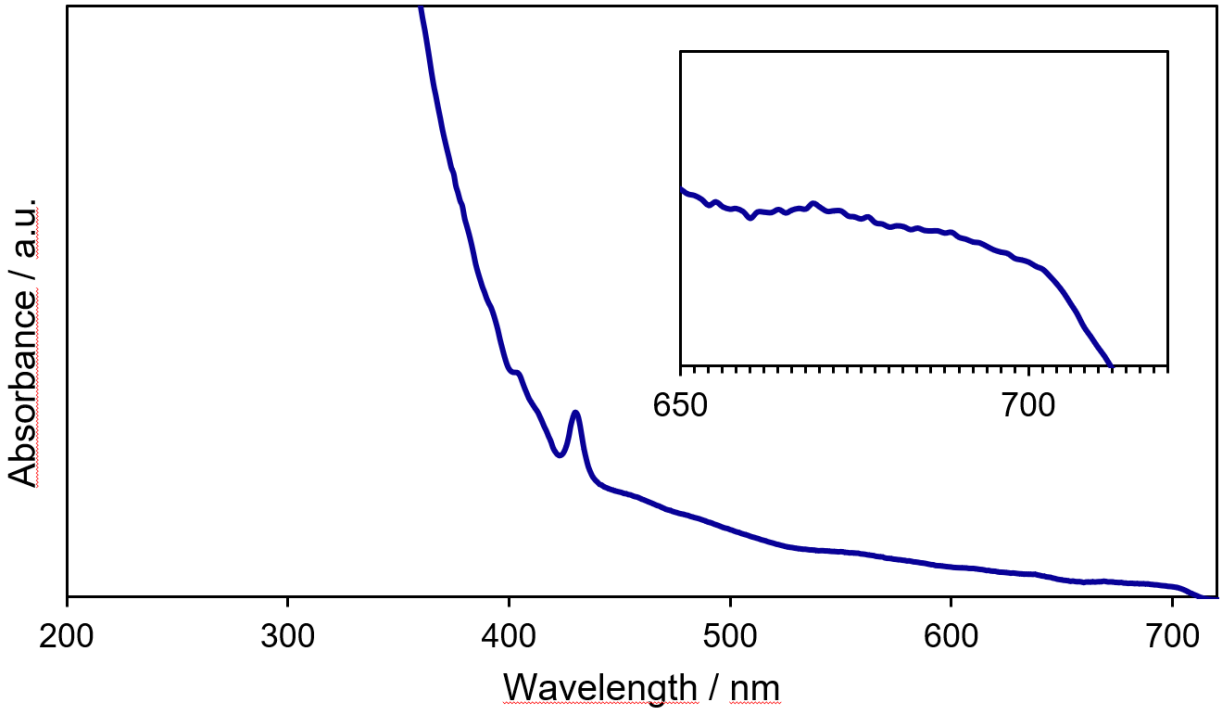

Figure S1. Absorption spectra (UV-Vis) of **1** in chloroform solution. Inset: zoom of the absorption spectrum of **1** between 650 and 720 nm.

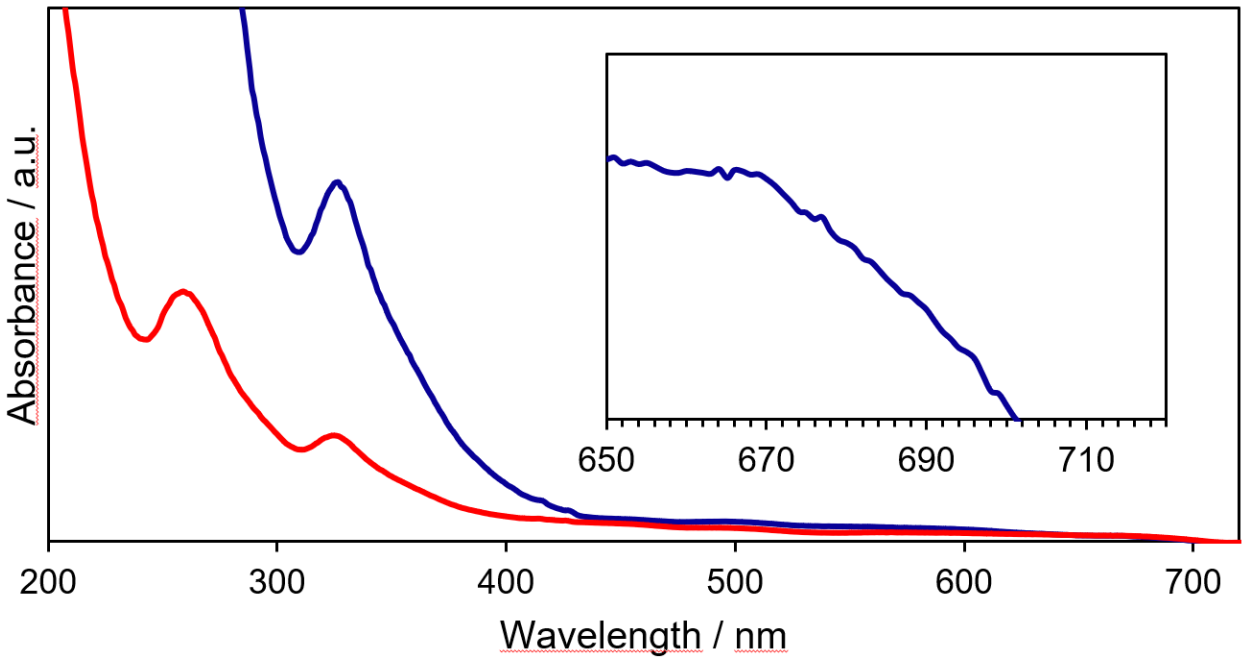

Figure S2. Absorption spectra (UV-Vis) of **2** in chloroform (blue line) and hexanes (red line) solution. Inset: zoom of the absorption spectrum of **2** in chloroform between 650 and 720 nm.

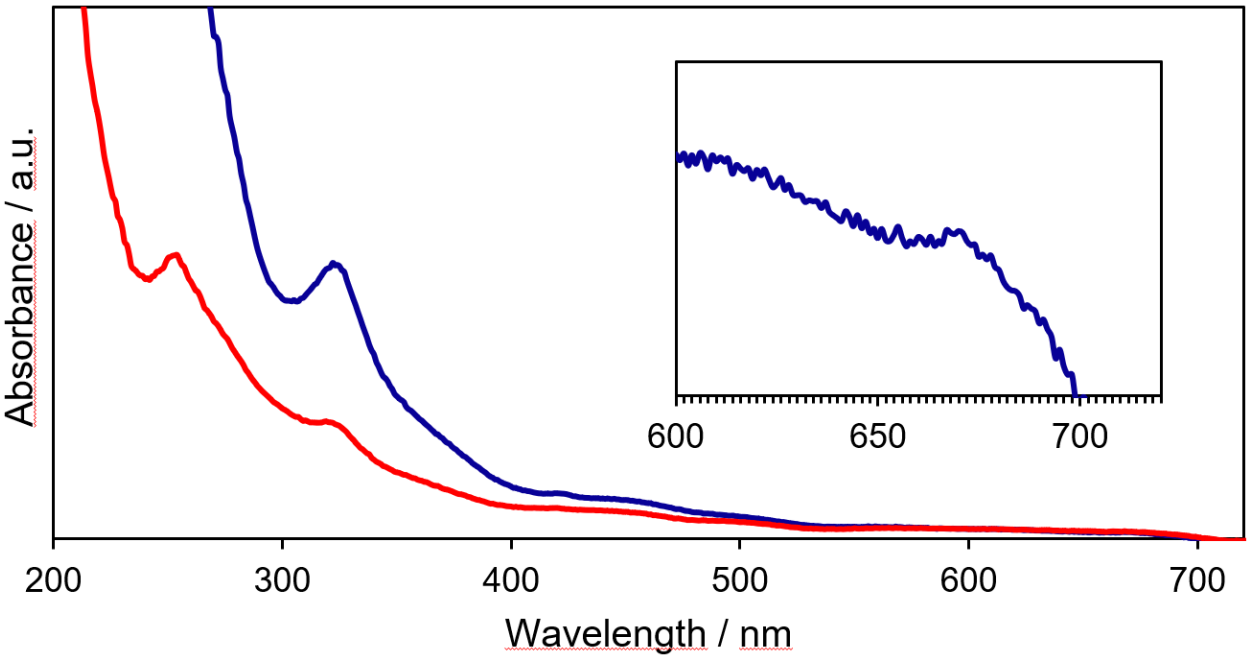

Figure S3. Absorption spectra (UV-Vis) of **3** in chloroform (blue line) and hexanes (red line) solution. Inset: zoom of the absorption spectrum of **3** in chloroform between 650 and 720 nm.

Electrochemical characterization of 1-3

Cyclic voltammetry (CV) for compounds **1**-**3** was carried out under an argon atmosphere at room temperature using a J-Cambria IH-660 potentiostat. Scan rate for CV experiments was 50 mV/s. A one compartment cell with a standard three-electrode set up was used, consisting of a 1 mm diameter glassy carbon disk as the working electrode, a platinum wire as the counter electrode and a silver wire as the pseudo-reference electrode, in a solution of anhydrous o-DCB containing 0.05 M *n*-Bu_4NPF_6. Ferrocene was used as internal Standard.

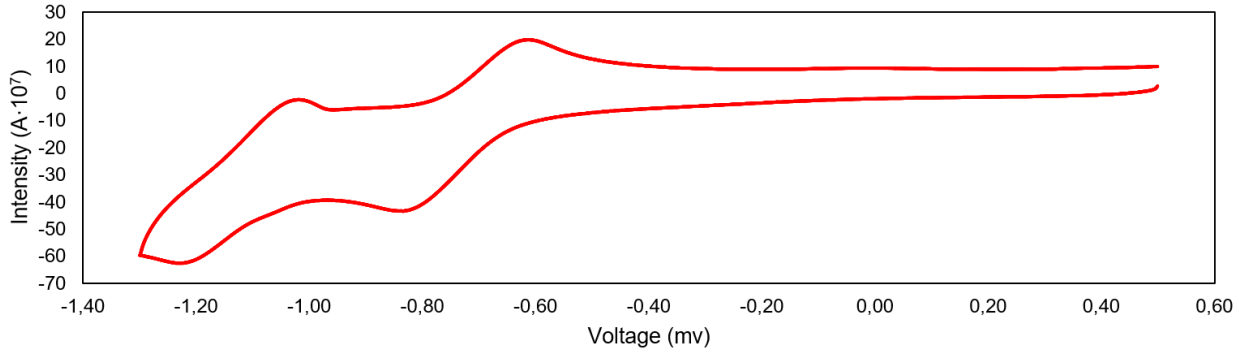

Figure S4. Cyclic voltammetry for **1** in *o*-DCB containing 0.05 M *n*-Bu_4NPF_6.

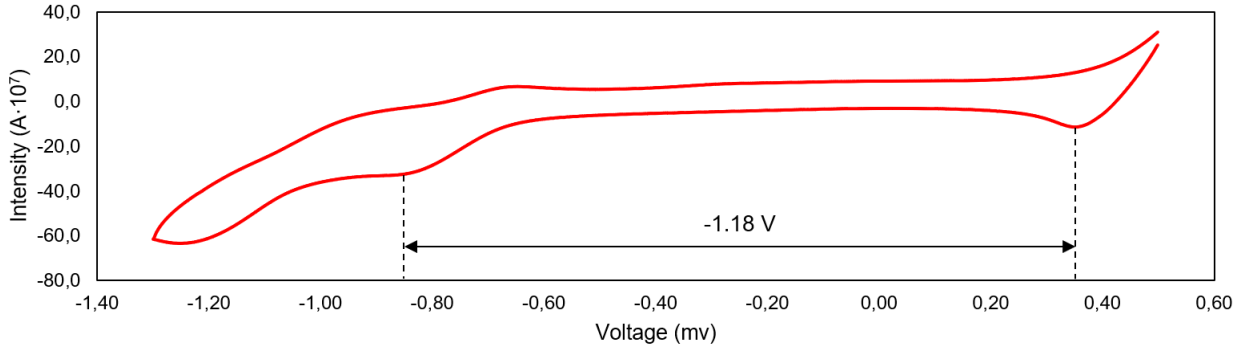

Figure S5. Cyclic voltammetry for **1** + ferrocene in *o*-DCB containing 0.05 M *n*-Bu_4NPF_6.

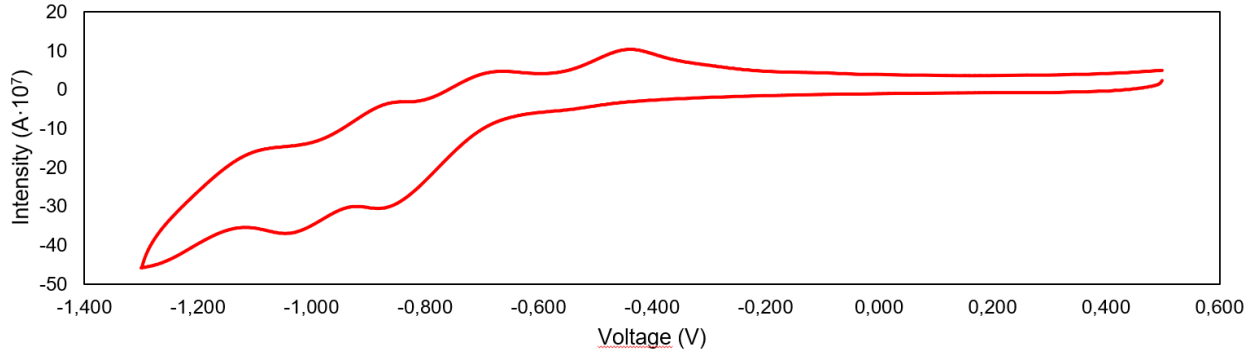

Figure S6. Cyclic voltammetry for **2** in *o*-DCB containing 0.05 M *n*-Bu_4NPF_6.

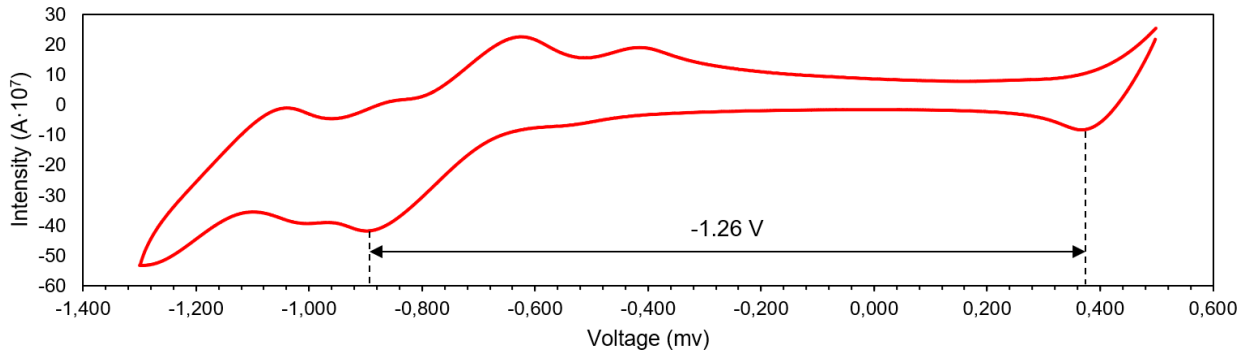

Figure S7. Cyclic voltammetry for **2** + ferrocene in *o*-DCB containing 0.05 M *n*-Bu_4NPF_6.

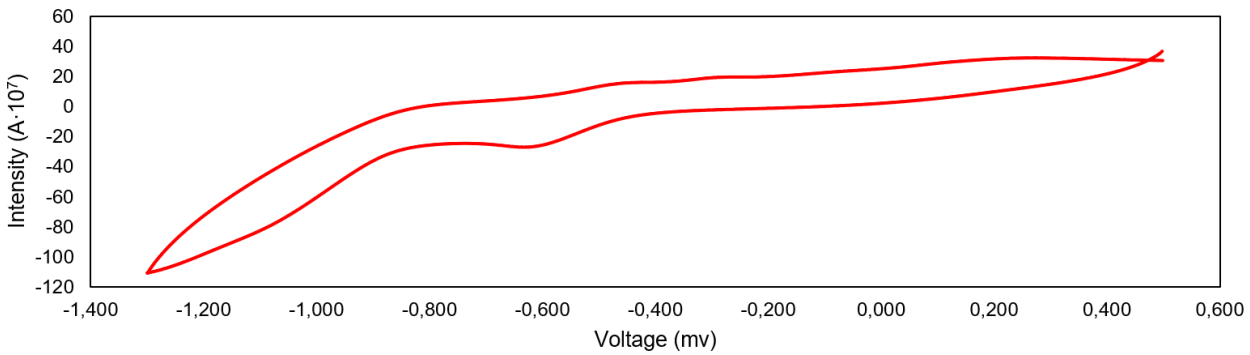

Figure S8. Cyclic voltammetry for **3** in *o*-DCB containing 0.05 M *n*-Bu_4NPF_6.

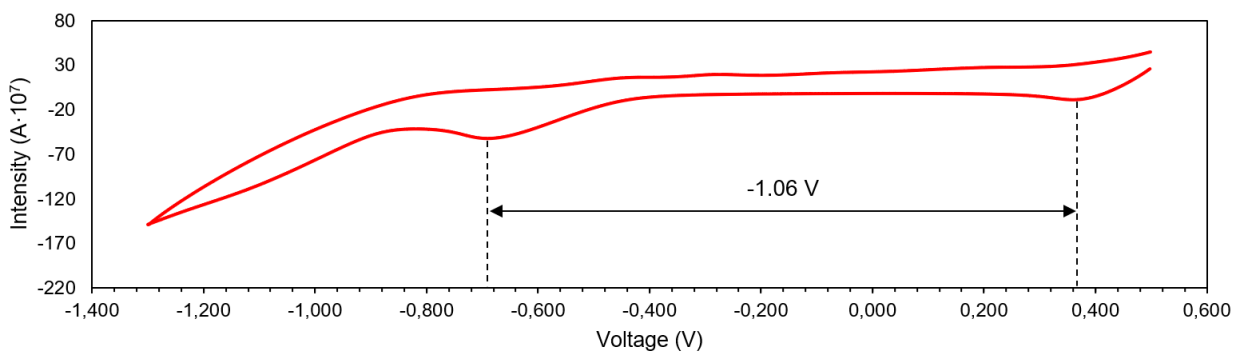

Figure S9. Cyclic voltammetry for **3** + ferrocene in *o*-DCB containing 0.05 M *n*-Bu_4NPF_6.

Table S1. Highest occupied molecular orbital/lowest unoccupied molecular orbital (HOMO/LUMO) values estimated from the ultraviolet (UV) and CV measurements.

Comp	λ_{max} (nm)	E_g (ev)	E_{red} (V)	LUMO (ev)	HOMO (ev)
1	712	1.74	-1.18	-3.62	-5.36
2	702	1.77	-1.26	-3.54	-5.31
3	699	1.77	-1.06	-3.74	-5.51

$E_{LUMO}=-(E_{red}+4.8\ eV)$
$E_{LUMO}=E_{HOMO}+E_g$
$E_g=1240/\lambda_{onset}$ (in eV)

Preparation of complexes of C_{60}, compound 1, 2, or 3 with PVP (preparation of C_{60}/PVP, P1, P2, or P3)

Compounds with PVP were prepared following the reported method.[5]

C_{60} / PVP. C_{60} (0.8 mg, 0.0011) was dissolved in toluene (1.0 mL) and added to 2.0 mL of $CHCl_3$ containing 100 mg of PVP (K-30). The resulting solution was sonicated for one hour and the solvent was then slowly evaporated under vacuum to afford **C_{60} / PVP**.

P1. Compound **1** (1.3 mg, 0.0013 mmol) was dissolved in toluene (1.0 mL) and added to 2.0 mL of $CHCl_3$ containing 106 mg of PVP (K-30). The resulting solution was sonicated for one hour and the solvent was then slowly evaporated under vacuum to afford **P1**.

P2. compound **2** (1.2 mg, 0.0011 mmol) was dissolved in toluene (1.0 mL) and added to 2.0 mL of $CHCl_3$ containing 103 mg of PVP (K-30). The resulting solution was sonicated for one hour and the solvent was then slowly evaporated under vacuum to afford **P2**.

P3. Compound **3** (1.3 mg, 0.0012 mmol) was dissolved in toluene (10. mL) and added to 2.0 mL of $CHCl_3$ containing 100 mg of PVP (K-30). The resulting solution was sonicated for one hour and the solvent was then slowly evaporated under vacuum to afford **P3**.

Absorption spectroscopic characterization of C_{60} and P1-P3

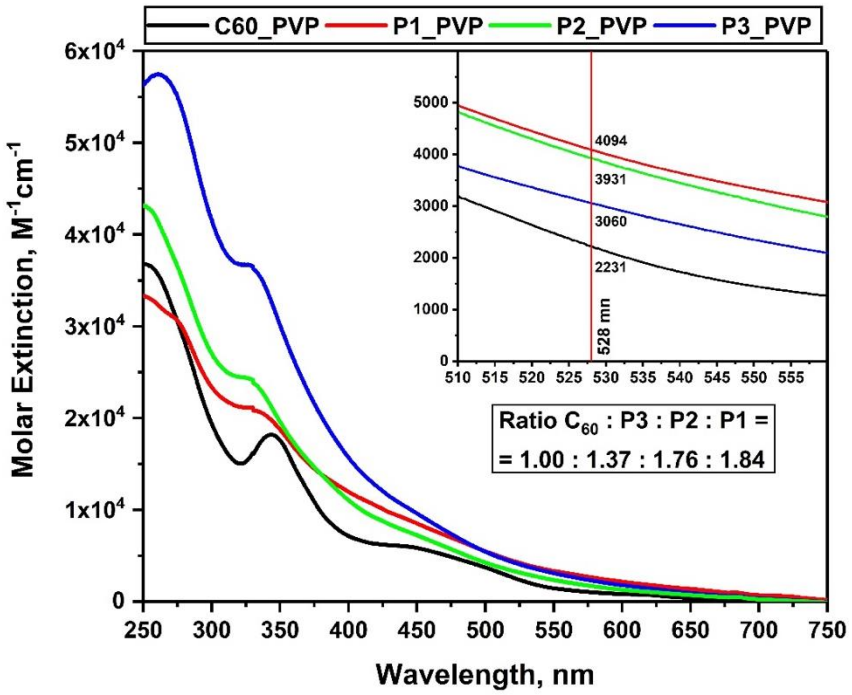

Figure S10. UV-Vis spectra of **C_{60}/PVP** and **P1-P3** conjugates in water with expansion (inset). ε = 2231, 4094, 3060, and 3931 $M^{-1}\cdot cm^{-1}$ at 528 nm for C_{60}, **P1**, **P2**, and **P3**, respectively.

Comparison of the absorption spectra of naked 1-3 derivatives and wrapped P1-P3 conjugates

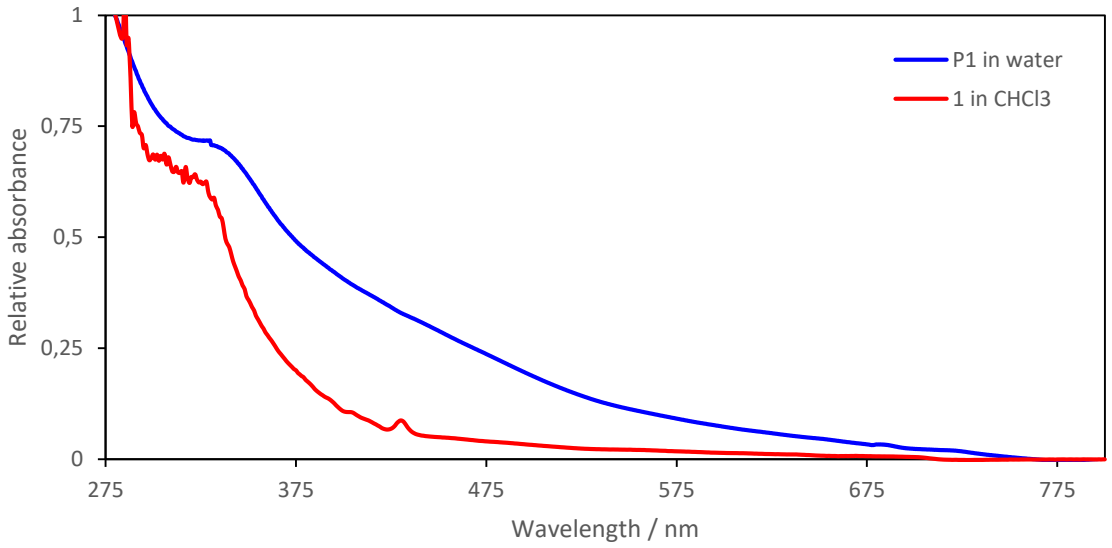

Figure S11. Comparison of the UV-Vis spectra of **1** in chloroform solution (red line) and **P1** in water solution (blue line).

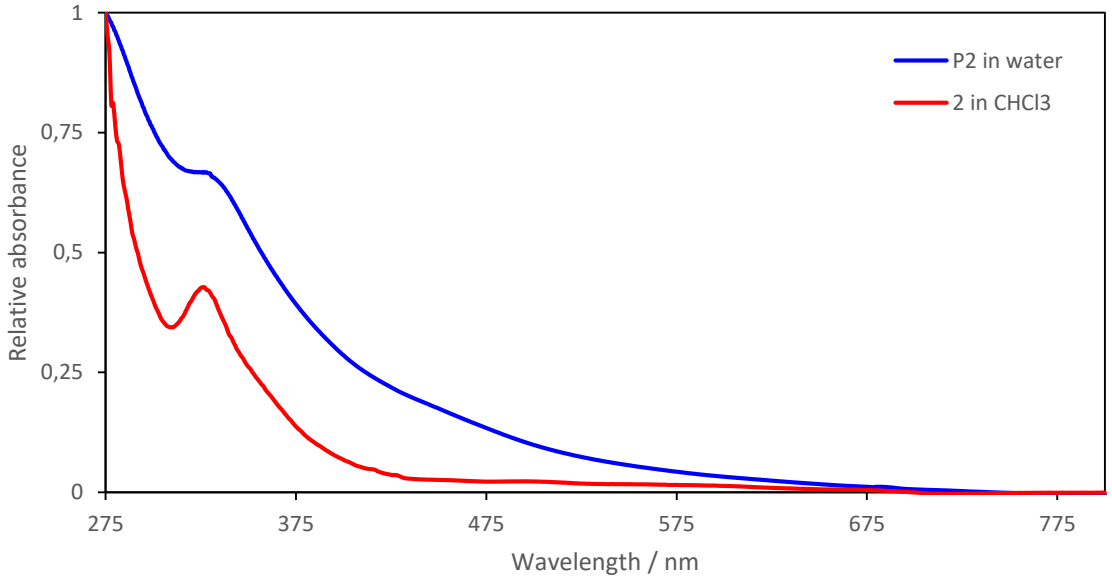

Figure S12. Comparison of the UV-Vis spectra of **2** in chloroform solution (red line) and **P2** in water solution (blue line).

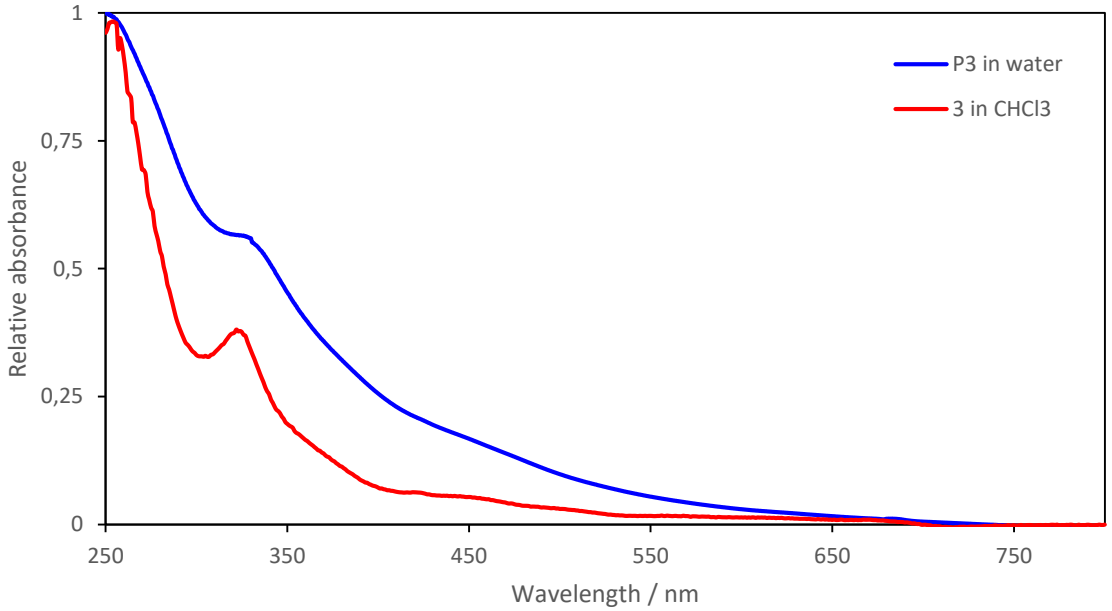

Figure S13. Comparison of the UV-Vis spectra of **3** in chloroform solution (red line) and **P3** in water solution (blue line).

ESR spin trapping experiments

ESR spectra were recorded on a Bruker EMX, Continuous Wave X-Band EPR spectrometer (Bruker BioSpin GmbH, Rheinstetten, Germany). Double integration of the spectra was performed using the WiNEPR Processing software (Bruker). Suprasil® ESR tubes with a diameter of 4 mm, length of 250 mm and a wall thickness of 0.8 mm were used (SP Wilmad-LabGlass, New Jersey, US). 50 µL Blaubrand® intraMark capillaries were bought from Brand (Brand GMBH, Wertheim, Germany). All aqueous solutions were prepared using milliQ water. 4-oxo-TEMP was purchased from ABCR (Karlsruhe, Germany) and purified by sublimation prior to use. DEPMPO was bought from Enzo Life Sciences AG (Farmingdale, NY, USA). L-Histidine, DETAPAC, DMSO and NADH were bought from Sigma-Aldrich (St. Louis, Missouri, USA). Irradiation was performed by green LED light (Lumitronix, PowerBar V3, true green, 528 nm, 93 lm•W^{-1}, 160 lamps in total) in a container with a diameter of 8.5 cm. All experiments were repeated 3 times independently. Double integration data is reported as mean of triplicate experiments.

$^1O_2$ generation

To a mixture of aqueous solution of each PVP complex C_{60} / PVP or **P1-3** (0.1 mM, 20 µL), aqueous solution of 4-oxo-TEMP (1 M, 4 µL), pH 7.0 phosphate buffer (300 mM, 10 µL), and milliQ water (16 µL), O_2 was bubbled in a 0.5 mL Eppendorf® tube for 45 sec. The solution was then taken into a 50 µL capillary and irradiated by the green LED. The capillary was then taken inside the ESR tube and subjected to the ESR measurement. Measurement conditions: temperature 298 K; microwave frequency 9.78 GHz; microwave power 10 mW; receiver gain 5.02 x 10^4; modulation amplitude 1.00 G; modulation frequency 100 KHz; sweep time 83.89 sec.

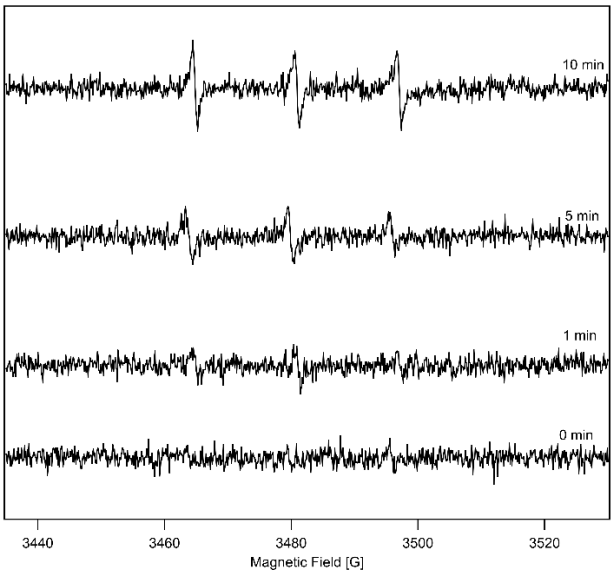

Figure S14. X-band ESR spectra of $^1O_2$ adduct of 4-oxo-TEMP generated in an aqueous solution of **C_{60}/PVP** under irradiation by 528 nm max LED. C_{60}/PVP: 40 µM; 4-oxo-TEMP: 80 mM; in 60 mM phosphate buffer (pH 7.0). Irradiation time: 0, 1, 5, 10 min.

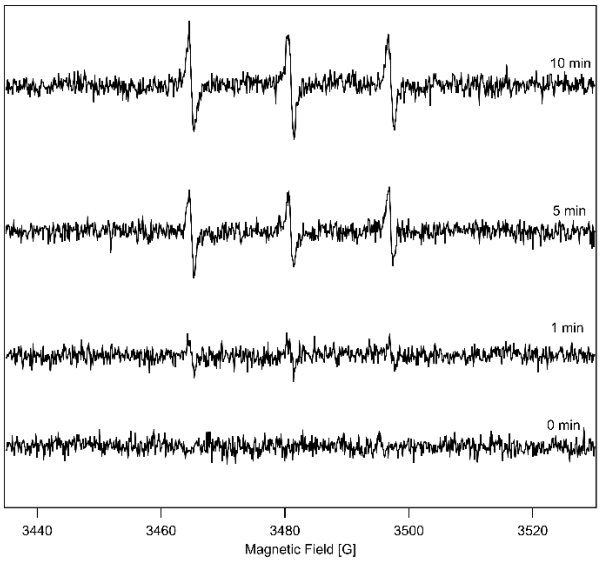

Figure S15. X-band ESR spectra of $^1O_2$ adduct of 4-oxo-TEMP generated in an aqueous solution of **P1** under irradiation by 528 nm max LED. **P1**: 40 µM; 4-oxo-TEMP: 80 mM; in 60 mM phosphate buffer (pH 7.0). Irradiation time: 0, 1, 5, 10 min.

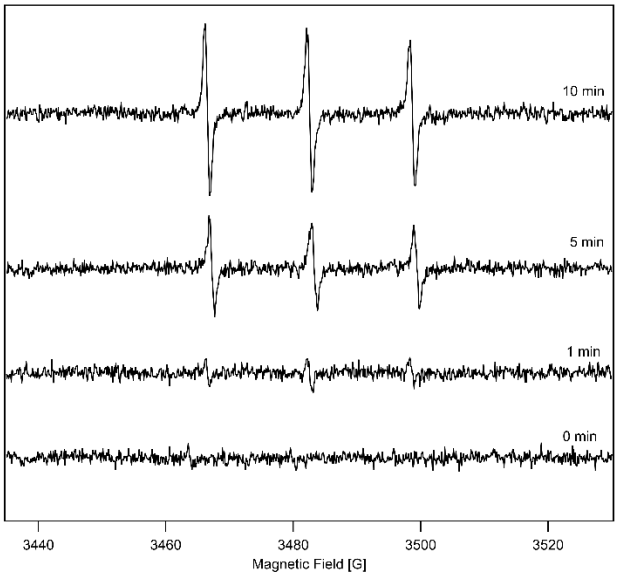

Figure S16. ESR spectra of $^1O_2$ adduct of 4-oxo-TEMP generated in an aqueous solution of **P2** under irradiation by 528 nm max LED. **P2**: 40 µM; 4-oxo-TEMP: 80 mM; in 60 mM phosphate buffer (pH 7.0). Irradiation time: 0, 1, 5, 10 min.

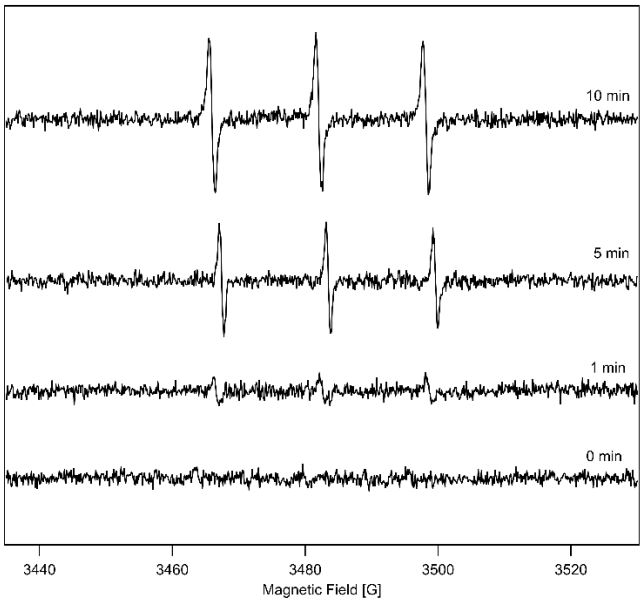

Figure S17. ESR spectra of $^1O_2$ adduct of 4-oxo-TEMP generated in an aqueous solution of **P3** under irradiation by 528 nm max LED. **P3**: 40 µM; 4-oxo-TEMP: 80 mM; in 60 mM phosphate buffer (pH 7.0). Irradiation time: 0, 1, 5, 10 min.

$O_2\bullet^-$ generation

To a mixture of aqueous solution of PVP complexes C_{60}/PVP or **P1-3** (0.1 mM, 20 µL), of DETAPAC solution in 0.3 M Phosphate Buffer (5 mM, 10 µL), aqueous solution of NADH (100 mM, 5 µL), aqueous solution of L-histidine (100 mM, 5 µL) and DEPMPO solution (565 mM, 10 µL) in DMSO O_2 was bubbled in a 0.5 mL Eppendorf® tube for 45 sec. The solution was then taken into a 50 µL capillary and irradiated by the green LED. The capillary was then taken inside the ESR tube and the measurement was performed. Measurement conditions: temperature 298 K; microwave frequency 9.78 GHz; microwave power 10 mW; receiver gain 5.02 x 10^4; modulation amplitude 1.00 G; modulation frequency 100 KHz; sweep time 83.89 sec. All experiments were repeated 3 times independently. Double integration data is reported as mean of triplicate experiments.

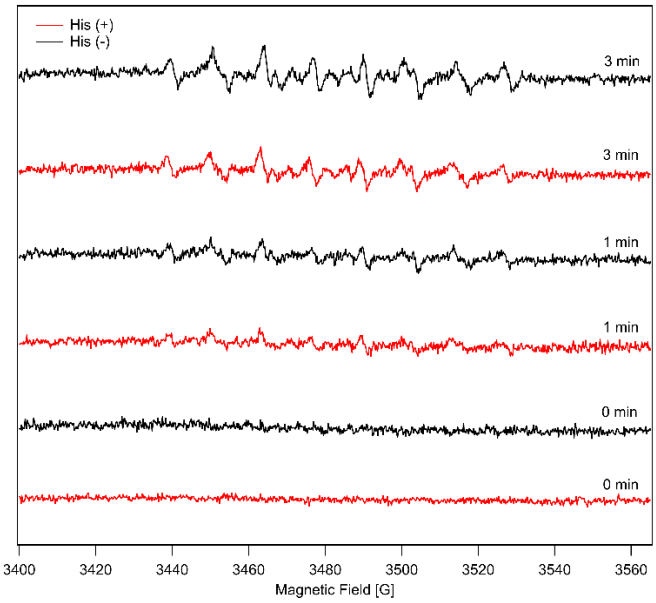

Figure S18. X-band ESR spectra of DEPMPO adduct with $O_2\bullet^-$ generated in an aqueous solution of C_{60}/PVP under irradiation by 528 nm max LED in the presence of L-histidine (black lines) and without L-histidine (red line). C60/PVP: 40 µM; DEPMPO: 113 mM; NADH: 10 mM; DETAPAC: 1 mM; L-histidine: 10 mM; in 60 mM phosphate buffer (pH 7.0) with 20% DMSO (v/v). Irradiation time: 0, 1, 3 min.

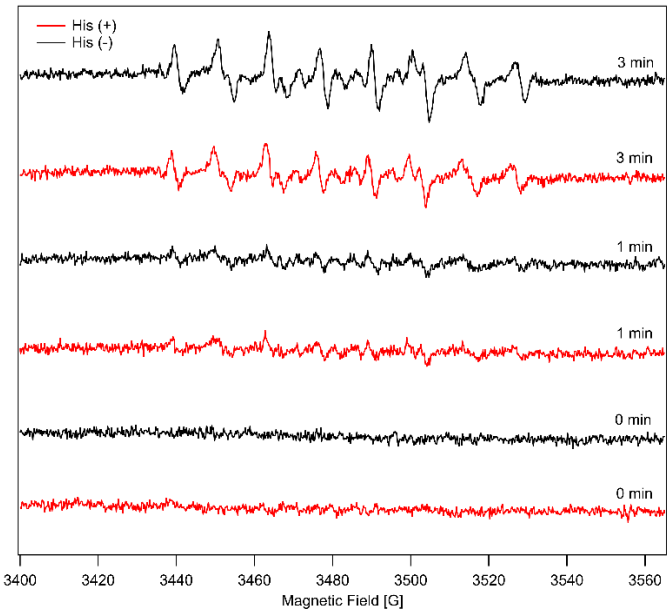

Figure S19. X-band ESR spectra of DEPMPO adduct with $O_2\bullet^-$ generated in an aqueous solution of **P1** under irradiation by 528 nm max LED in the presence of L-histidine (black lines) and without L-histidine (red line). **P1**: 40 µM; DEPMPO: 113mM; NADH: 10 mM; DETAPAC: 1 mM; L-histidine: 10 mM; in 60 mM phosphate buffer (pH 7.0) with 20% DMSO (v/v). Irradiation time: 0, 1, 3 min.

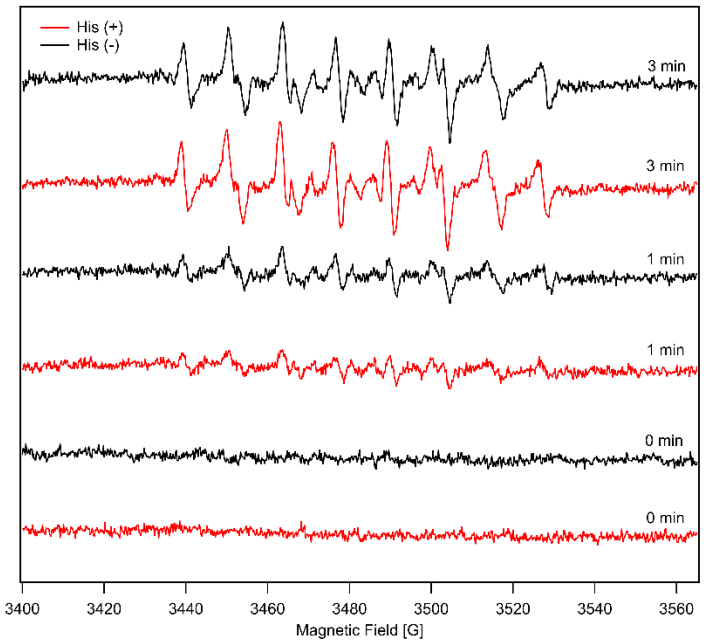

Figure S20. X-band ESR spectra of DEPMPO adduct with $O_2^{\bullet-}$ generated in an aqueous solution of **P2** under irradiation by 528 nm max LED in the presence of L-histidine (black lines) and without L-histidine (red line). **P2**: 40 µM; DEPMPO: 113 mM; NADH: 10 mM; DETAPAC: 1 mM; L-histidine: 10 mM; in 60 mM phosphate buffer (pH 7.0) with 20% DMSO (v/v). Irradiation time: 0, 1, 3 min.

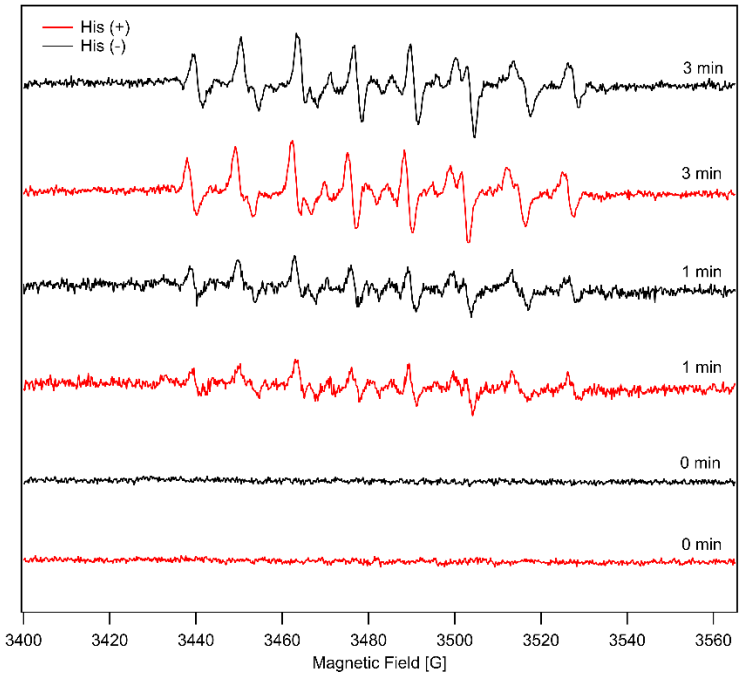

Figure S21. X-band ESR spectra of DEPMPO adduct with $O_2^{\bullet-}$ generated in an aqueous solution of **P3** under irradiation by 528 nm max LED in the presence of L-histidine (black lines) and without L-histidine (red line). **P3**: 40 µM; DEPMPO: 113 mM; NADH: 10 mM; DETAPAC: 1 mM; L-histidine: 10 mM; in 60 mM phosphate buffer (pH 7.0) with 20% DMSO (v/v). Irradiation time: 0, 1, 3 min.

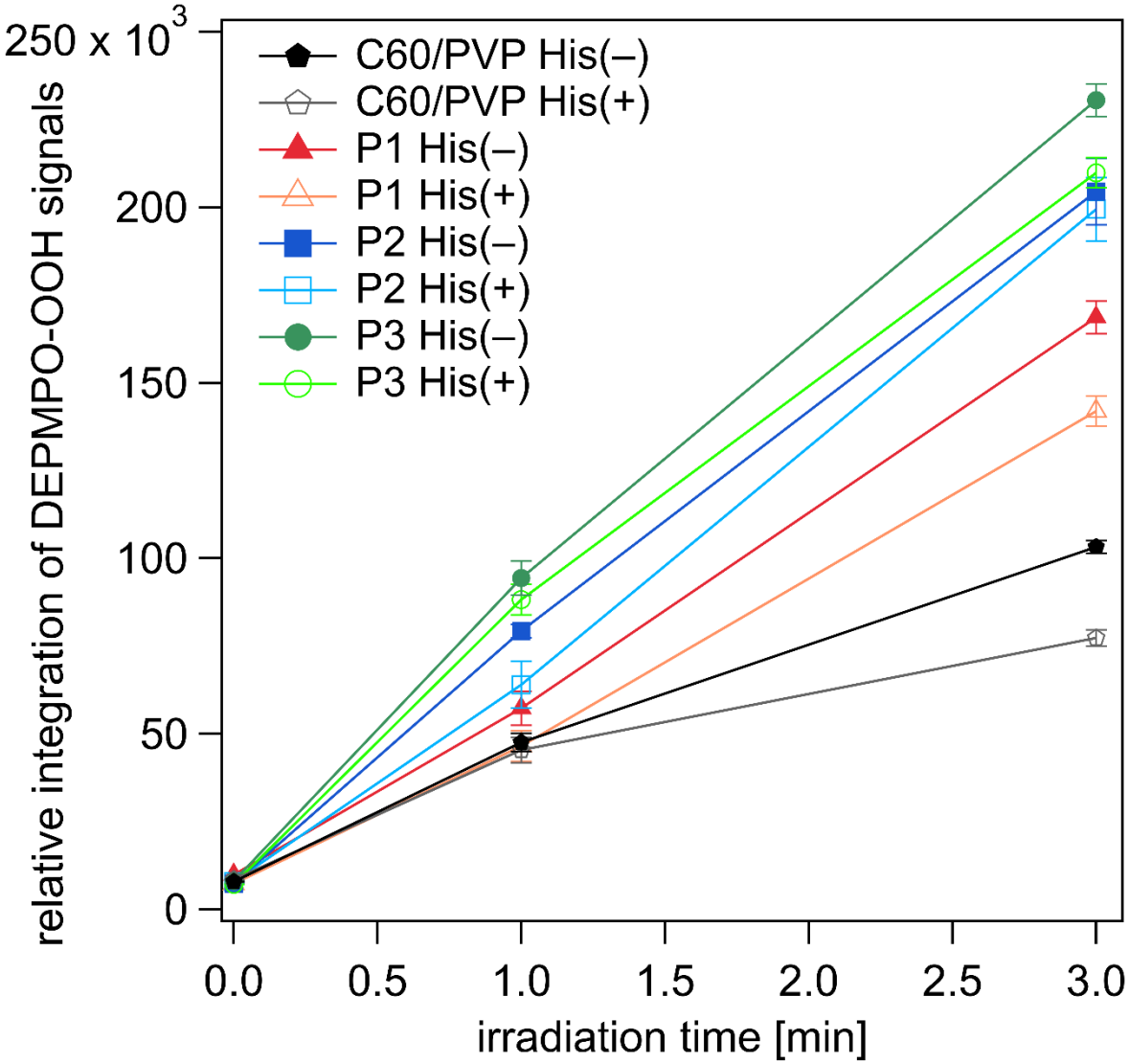

Figure S22. Time-dependent generation of $O_2\bullet^-$ measured by double-integration of ESR signals corresponding to $O_2\bullet^-$ adduct of DEPMPO (DEPMPO-OOH) generated in aqueous solutions C_{60}/PVP and **P1-3** in the absence or presence of L-histidine under irradiation by green LED (528 nm max). Error bars indicate standard deviation (n=3).

DNA Photocleavage Assay

The pBR322 DNA and Gel Loading Dye, Purple (6X) were bought from New England Biolabs (Ipswich, Massachusetts, USA). Nunc MicroWell 96 Well Round (U) Bottom Plate was bought from Thermo Scientific (Waltham, Massachusetts, U.S). Ethylenediaminetetraacetic acid disodium salt dihydrate (EDTA), β-Nicotinamide adenine dinucleotide reduced disodium salt hydrate (NADH), GelRed® Nucleic Acid Stain 10000X and agarose were bought from Sigma-Aldrich (St. Louis, MI, USA). Lumidox® II 96-well LED Array equipped with 527 nm max (Analytical Sales and Services, Inc., New Jersey, USA) was used for light irradiation. Gel Electrophoreses were performed using Mupid-exU gel electrophoresis system (Mupid CO. LTD., Tokyo, JAPAN). Imaging of the gels were performed using ChemiDoc Imaging System (Bio-Rad Laboratories, Inc., CA, USA).

The pBR322 DNA was diluted to a stock solution of 50 ng/µL, in Tris/HCl buffer (pH 8.0, 1 mM EDTA). 10 µL of the DNA solution was mixed with 5 µL of **P1-3** or C_{60}/PVP solution (0.5 mM) in Tris/HCl and 5 µL of NADH (40 mM) in Tris/HCl. The mixtures were irradiated by 96-well illuminator for 25 min using 527 nm max light source and 45 mW power setting. 4 µL of Gel Loading Dye, Purple (6X) were added into the wells and all contents were loaded in an agarose gel prepared by 0.5X TBE buffer and 1% agarose. Electrophoreses were conducted at 100V for 80 min using 0.5X TBE as the running buffer. The gel was then stained using GelRed® Nucleic Acid Stain 10000X diluted to 3X in milliQ water for 1 hour. The gels were then imaged using GelRed filter settings to produce the images. The images were analyzed using ImageJ software.

Sample	0	0	0	0	P2	P2	P2	P2	P3	P3	P3	P3
NADH	+	-	+	-	+	-	+	-	+	-	+	-
Light	+	+	-	-	+	+	-	-	+	+	-	-

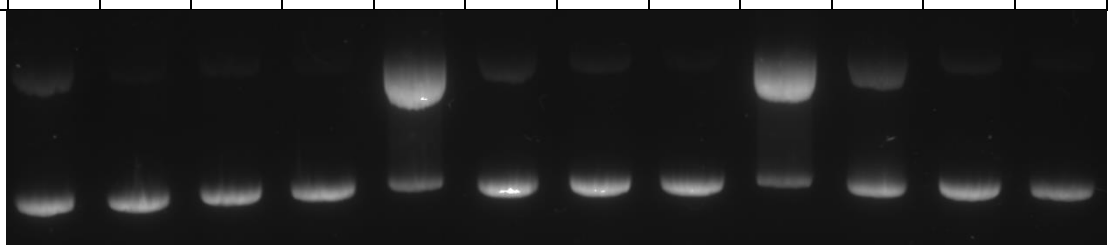

Figure S23. Photoinduced DNA cleavage by **P2** and **P3**. The pBR322 supercoiled plasmid was incubated with each compound under photoirradiation. Reaction conditions: pBR322: 25 ng·μL^{-1}; **P2** or **P3**: 0.125 mM; NADH: 10 mM; in Tris-HCl buffer (pH 8.0, 1 mM EDTA); green LED (527 nm, 45 lm·W^{-1}), at room temperature, for 25 min. Electrophoresis: 100 V, 80 min, 1% agarose in 0.5X TBE buffer (pH 8.3).

Sample	0	0	0	0	C_{60}	C_{60}	C_{60}	C_{60}	P1	P1	P1	P1
NADH	+	-	+	-	+	-	+	-	+	-	+	-
Light	+	+	-	-	+	+	-	-	+	+	-	-

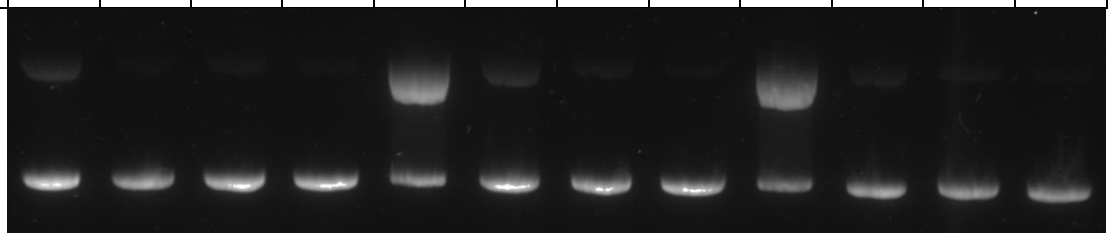

Figure S24. Photoinduced DNA cleavage by C_{60}/PVP and **P1**. The pBR322 supercoiled plasmid was incubated with each compound under photoirradiation. Reaction conditions: pBR322: 25 ng·μL^{-1}; C_{60}/PVP or **P1**: 0.125 mM; NADH: 10 mM; in Tris-HCl buffer (pH 8.0, 1 mM EDTA); green LED (527 nm, 45 lm·W^{-1}), at room temperature, for 25 min. Electrophoresis: 100 V, 80 min, 1% agarose in 0.5X TBE buffer (pH 8.3).

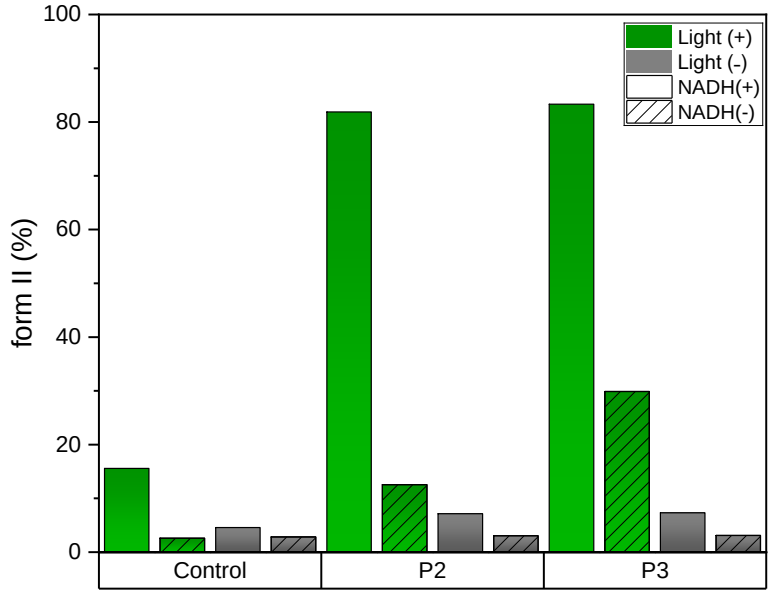

Figure S25. Relative amount of nicked form II of **P2** and **P3**.

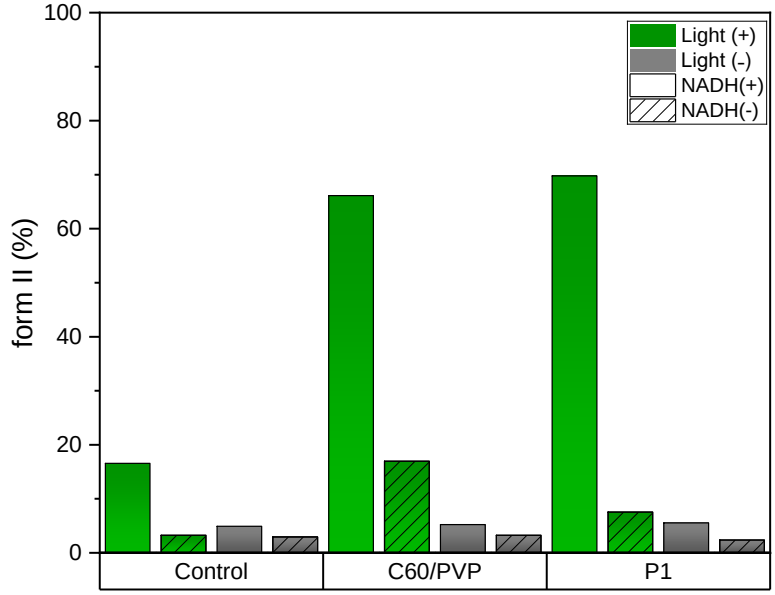

Figure S26. Relative amount of nicked form II of C_{60} and **P1**.

Quantum-chemical calculations

Geometry optimization of the complexes was performed employing the DFT range-separated CAM-B3LYP[6] functional with Ahlrichs' def2-SVP basis set.[7,8] The empirical dispersion D3 correction was computed with the Becke–Johnson damping function.[9,10] Excitation energies were calculated with the same functional and basis set using Tamn-Dancoff approximation (TDA) formalism.[11] Calculations were performed with the Gaussian 16 (rev. A03) and Orca 5.0.3 programs.[12-14] Molecular structures and frontier molecular orbitals were visualized by Chemcraft 1.8. program.[15]

Analysis of excited states

The quantitative analysis of exciton delocalization and charge transfer in the donor-acceptor complexes was carried out in terms of the transition density.[16-18] The analysis was done in the Löwdin orthogonalized basis, which is more convenient. The matrix ${}^{\lambda}\mathbf{C}$ of orthogonalized MO coefficients is obtained from the coefficients **C** in the original basis ${}^{\lambda}\mathbf{C} = \mathbf{S}^{1/2}\,\mathbf{C}$, where **S** is the atomic orbital overlap matrix. The transition density matrix T^{0i} for an excited state Φ_i^* constructed as a superposition of singly excited configurations (where an occupied MO ψ_j is replaced a virtual MO ψ_a) is computed as,

$$T^{0i}_{\alpha\beta} = \sum_{ja} A_{j\to a}\, {}^{\lambda}C_{\alpha j}\, {}^{\lambda}C_{\beta a} \tag{1}$$

where $A_{j\to a}$ is the expansion coefficient.

A key quantity Ω (D,A) is determined by:

$$\Omega(D,A) = \sum_{\alpha\in D,\,\beta\in A} \left(T^{0i}_{\alpha\beta}\right)^2 \tag{2}$$

The weights of local excitations on donor (D) and acceptor (A) are Ω(D,D) and Ω(A,A). The weights of electron transfer configurations D→A and A→D are represented by Ω(D,A) and Ω(A,D), respectively. The index Δq, which describes charge separation and charge transfer between D and A, is

$$\Delta q(CS) = \sum \Omega(D,A) - \Omega(A,D) \tag{3}$$

$$\Delta q(CT) = \sum \Omega(D,A) + \Omega(A,D) \tag{4}$$

Solvent Effects

The equilibrium solvation energy E_S^{eq} of a molecule (in the ground or excited state) in the medium with the dielectric constant ε was estimated using a COSMO-like polarizable continuum model[19-23] in the monopole approximation:

$$E_S^{eq}(Q,\varepsilon) = -\frac{1}{2} f(\varepsilon) Q^{+} D Q \tag{5}$$

where the $f(\varepsilon)$ is the dielectric scaling factor, $f(\varepsilon)=\frac{\varepsilon-1}{\varepsilon}$, **Q** – the vector of *n* atomic charges in the molecular system, **D** is the *n* x *n* symmetric matrix determined by the shape of the boundary surface between solute and solvent. $\mathbf{D}=\mathbf{B}^{+}\mathbf{A}^{-1}\mathbf{B}$, where the *m* x *m* matrix **A** describes electrostatic interaction between *m* surface charges and the *m* x *n* **B** matrix describes the interaction of the surface charges with *n* atomic charges of the solute.[19,23] The GEPOL93 scheme[24] was used to construct the molecular boundary surface.

The charge on atom X in the excited state Φ_i*, q_X^i, was calculated as:

$$q_X^i = q_X^0 + \Delta_X^i, \quad \Delta_X^i = \sum_{Y\neq X}\sum_{\alpha\in X,\,\beta\in Y}(T_{\alpha\beta}^{0i}T_{\alpha\beta}^{0i} - T_{\beta\alpha}^{0i}T_{\beta\alpha}^{0i}), \tag{6}$$

where q_X^0 is the atomic charge on A in the ground state and Δ_X^i is its change due to the redistribution of the electron density between the atoms X and the rest of atoms Y, which is caused by the excitation $\psi_0 \rightarrow \Phi_i$*.

The non-equilibrium solvation energy for excited state Φ_i*can be estimated as:[25]

$$E_S^{neq}(Q^0,\Delta,\varepsilon,n^2) = f(\varepsilon)\Delta^{+}DQ^0 - \frac{1}{2}f(n^2)\Delta^{+}D\Delta, \tag{7}$$

In Eq. (7), n^2 (the refraction index squared) is the optical dielectric constant of the medium and the vector Δ describes the change of atomic charges in the molecule by excitation in terms of atomic charges, see Eq. (6). By definition, the external (solvent) reorganization energy is the difference of the non-equilibrium (Eq. 7) and equilibrium (Eq. 5) solvation energies of the excited state.

Electron transfer rates

The rate of the nonadiabatic electron transfer (ET), k_{ET}, can be expressed in terms of the electronic coupling squared, V^2, and the Franck-Condon Weighted Density of states (FCWD):

$$k_{ET} = \frac{2\pi}{\hbar}V^2\,(FCWD) \tag{8}$$

that accounts for the overlap of vibrational states of donor and acceptor and can be approximately estimated using the classical Marcus equation:[26]

$$(FCWD) = (4\pi\lambda kT)^{-1/2}\exp\left[-(\Delta G^0+\lambda)^2/4\lambda kT\right] \tag{9}$$

where λ is the reorganization energy and ΔG^0 is the standard Gibbs energy change of the process.

Reorganization energy

The reorganization energy is usually divided into two parts, $\lambda = \lambda_i + \lambda_s$, including the internal and solvent terms. The solvent reorganization energy corresponds to the energy required to move solvent molecules from the position they occupy in the initial state to the location they have in the CT state, but without charge transfer having occurred. The λ_s for a particular CT state was computed as a difference between the equilibrium (E_s^{eq}, see eq. 5) and non-equilibrium (E_s^{neq}, see eq. 7) solvation energies. The internal

reorganization energy λ_i corresponds to the energy of structural changes when donor/acceptor fragments going from initial-state geometries to final-state geometries.

Table S2. Energies of lowest-lying S_1 and T_1 excited states estimated in Frank-Condon ($^{\neq}$) and relaxed ($^{=}$) geometries.

System	Lowest $S_1^{\neq}$	Lowest $S_1^{=}$	ΔS_1 [a]	Lowest $T_1^{\neq}$	Lowest $T_1^{=}$	ΔT_1[a]
1	2.426	1.942	0.484	1.991	1.507	0.484
2	2.590	2.006	0.584	2.017	1.563	0.454
3	2.534	1.905	0.629	1.964	1.378	0.586
C_{60}	2.637	2.024	0.613	2.045	1.564	0.481

[a] $\Delta S_1 = S_1^{\neq} - S_1^{=}$; $\Delta T_1 = T_1^{\neq} - T_1^{=}$;

Table S3. Gibbs energy ΔG^0, and total reorganization energy λ_t, for ISC *type II*, and *type I* reactions, computed in water for systems **P1**-**P3** and C_{60} fullerene.

System	ΔG^0, eV	λ_t, eV	$\Delta G^0 + \lambda_t$, eV
	Intersystem crossing reaction: $^1(P_X^*) \rightarrow {}^3(P_X^*)$		
1	-0.435	0.090	-0.345
2	-0.443	0.334	-0.109
3	-0.527	0.287	-0.240
C_{60}	-0.460	0.049	-0.411
	Type II reaction: $^3(P_X^*) + {}^3\Sigma_g^-(O_2) \rightarrow {}^1(P_X) + {}^1\Delta_g(O_2)$		
1	-0.530	0.433	-0.097
2	-0.586	0.549	-0.037
3	-0.401	0.496	0.095
C_{60}	-0.587	0.305	-0.282
	Type I, part1 reaction: $^3(P_X^*) + NADH \rightarrow (P_X)^{-\bullet} + NADH^{+\bullet}$		
1	-0.598	1.016	0.418
2	-0.439	1.023	0.584
3	-0.514	0.926	0.412
C_{60}	-0.726	0.999	0.273
	Type I, part2 reaction: $(P_X)^{-\bullet} + {}^3\Sigma_g^-(O_2) \rightarrow {}^1(P_X) + O_2^{-\bullet}$		
1	-0.875	1.170	0.295
2	-0.923	1.153	0.230
3	-0.674	1.159	0.485
C_{60}	-0.845	1.290	0.445

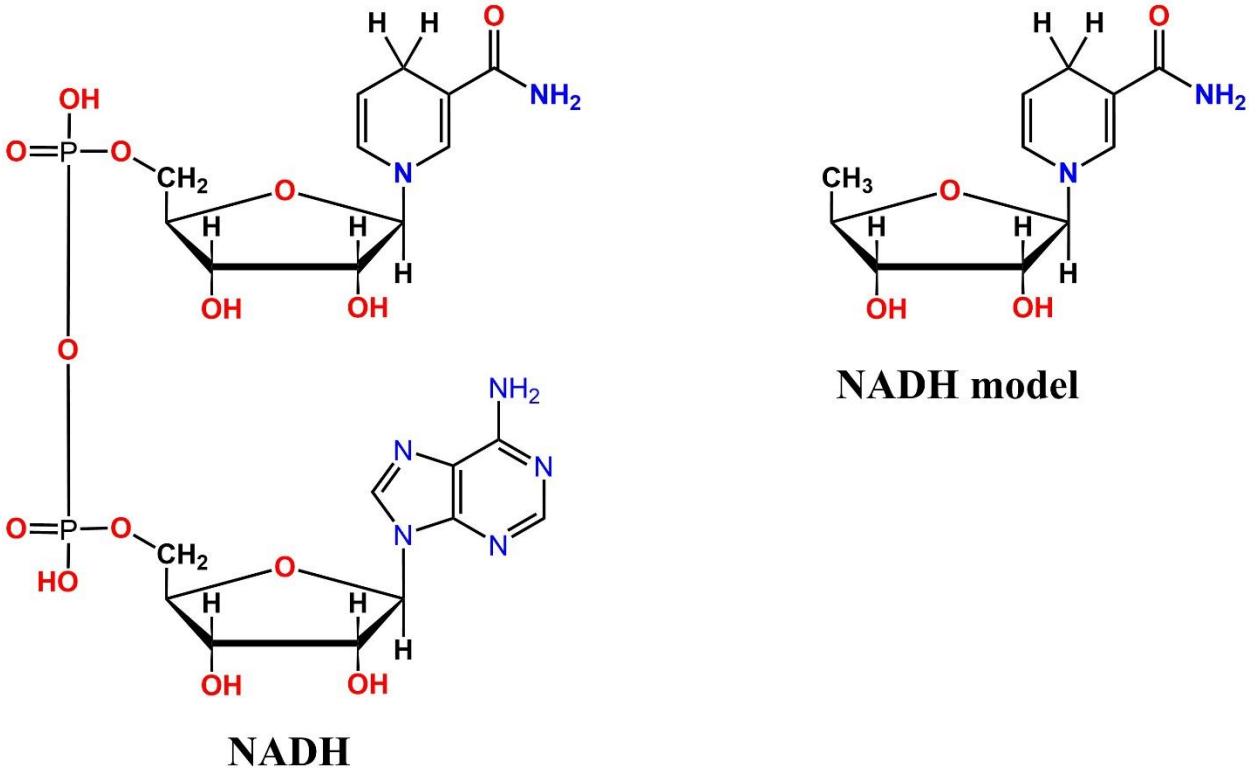

Figure S27. Graphical representation of NADH and used in this work NADH model.

^{1}H NMR, ^{13}C NMR and mass spectra

Compound 1

^{1}H NMR (400 MHz, $CDCl_3$, 298 K)

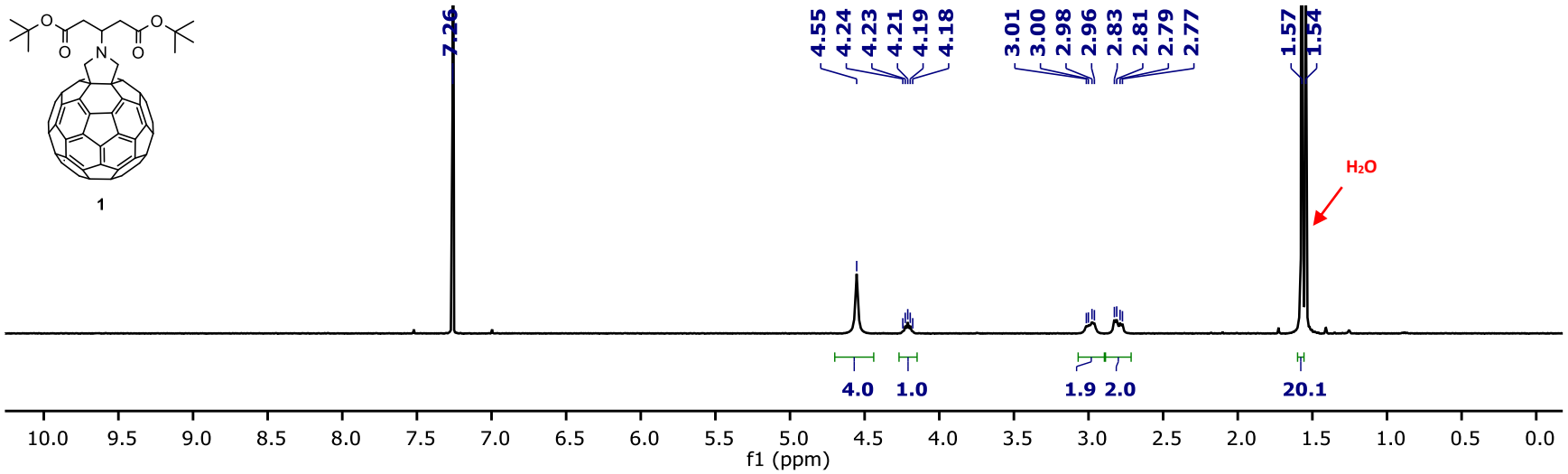

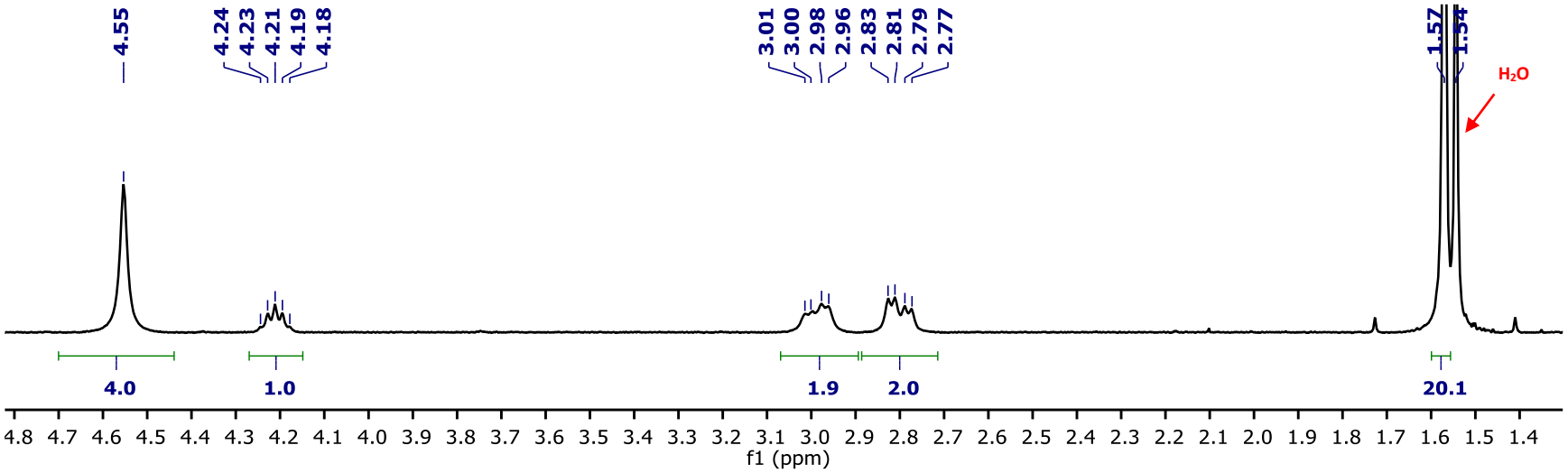

^{13}C NMR (150 MHz, $CDCl_3$)

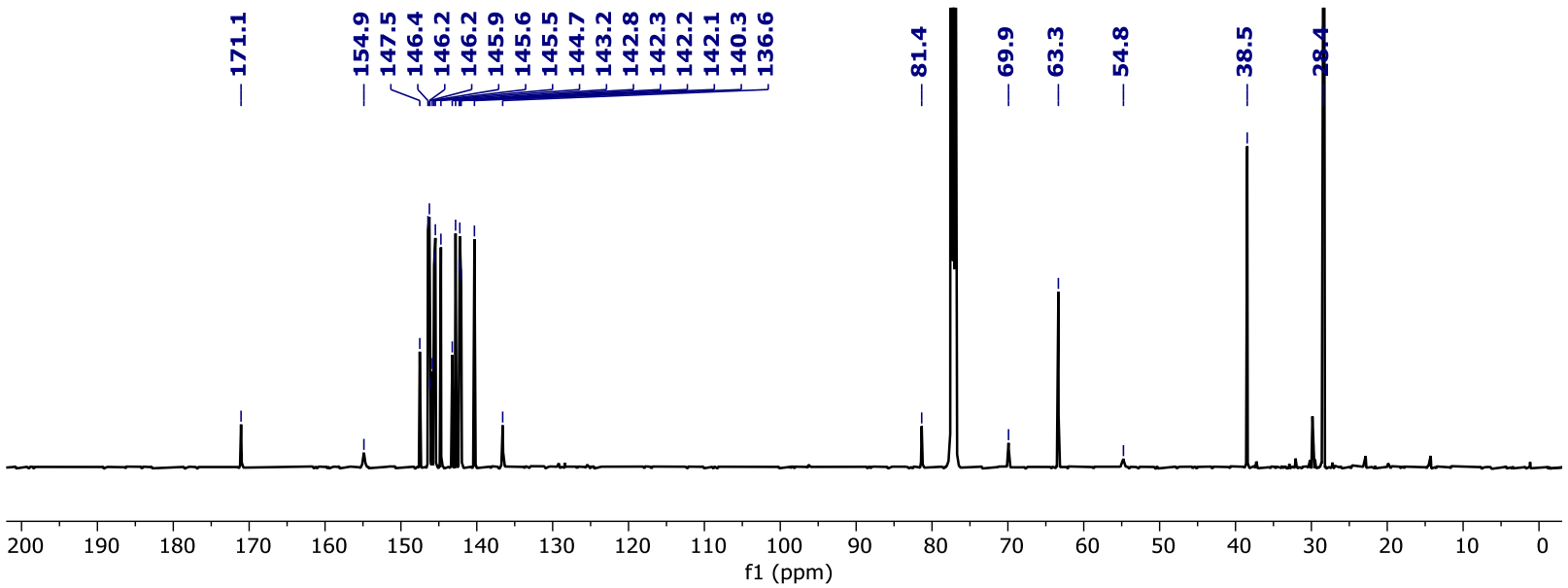

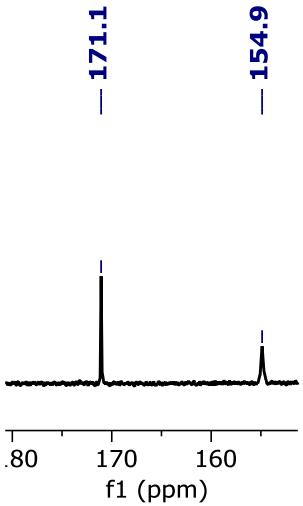

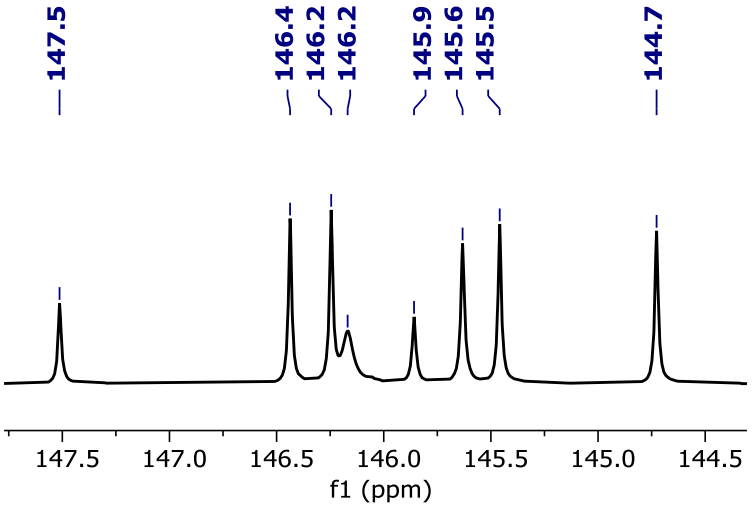

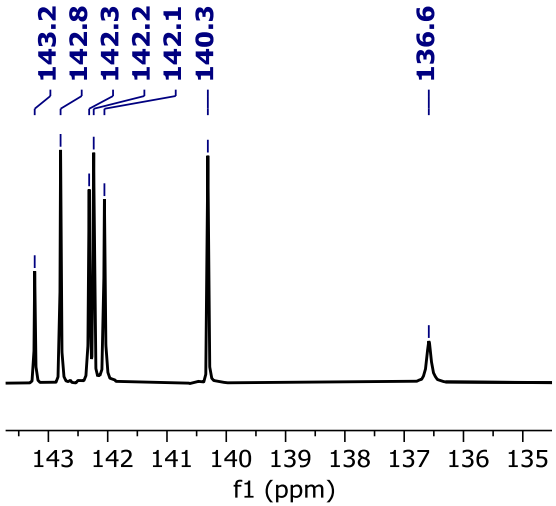

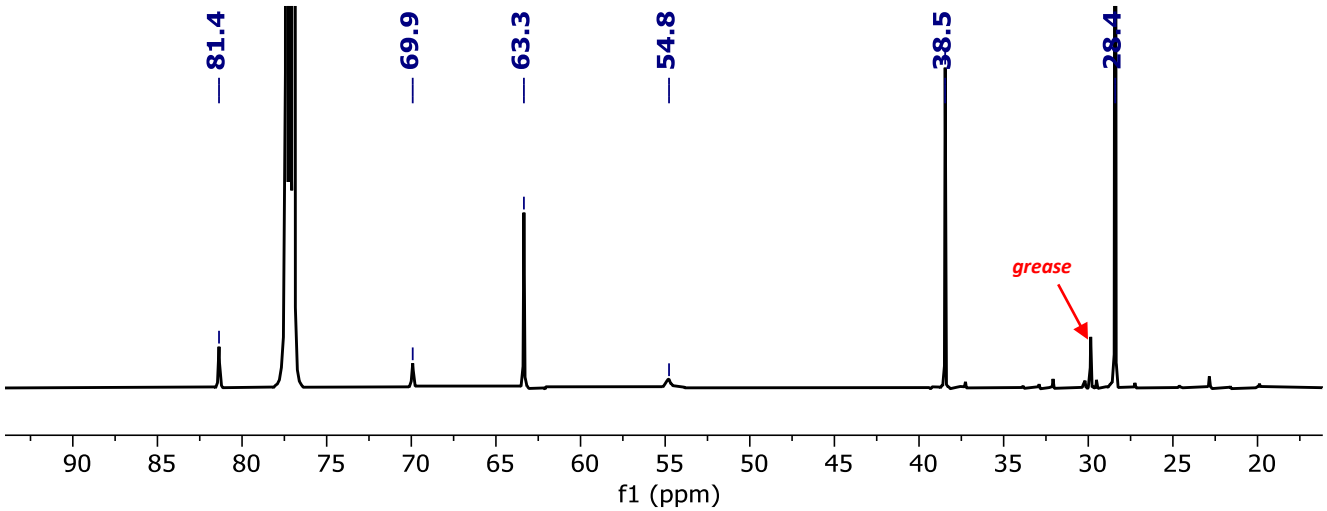
81.4
69.9
63.3
54.8
38.5
28.4
grease
90 85 80 75 70 65 60 55 50 45 40 35 30 25 20
f1 (ppm)

ESI-MS

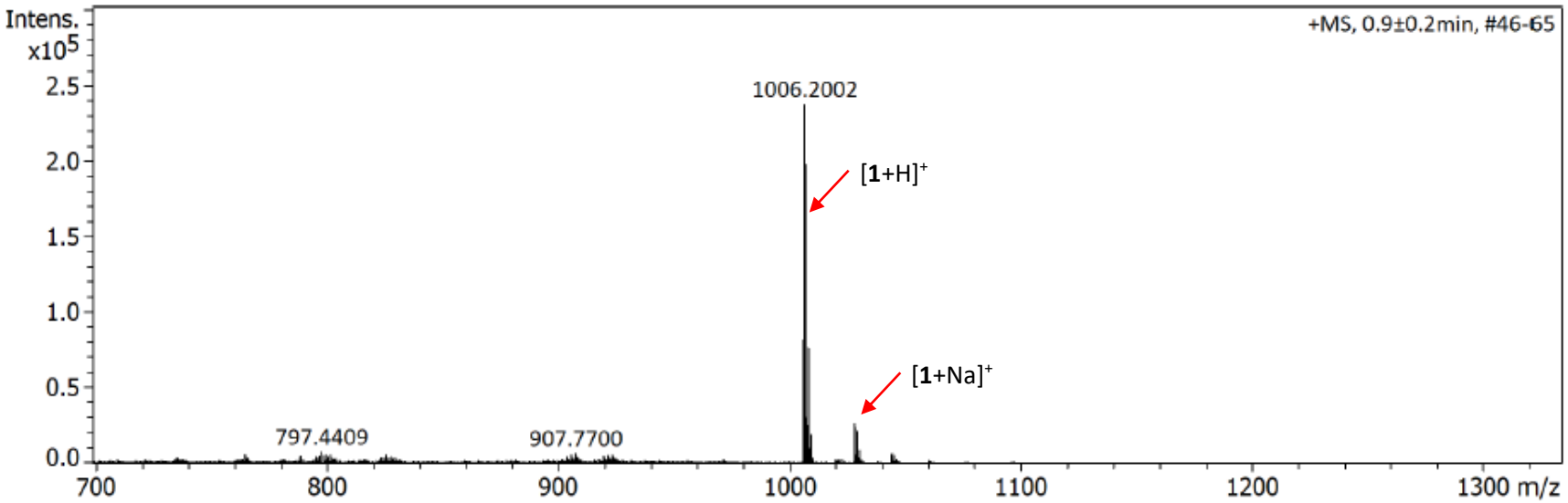
Intens.
x10^5
+MS, 0.9±0.2min, #46-65
1006.2002
[1+H]+
[1+Na]+
797.4409
907.7700
2.5
2.0
1.5
1.0
0.5
0.0
700 800 900 1000 1100 1200 1300 m/z

Compound 2

^{1}H NMR (400 MHz, $CDCl_3$)

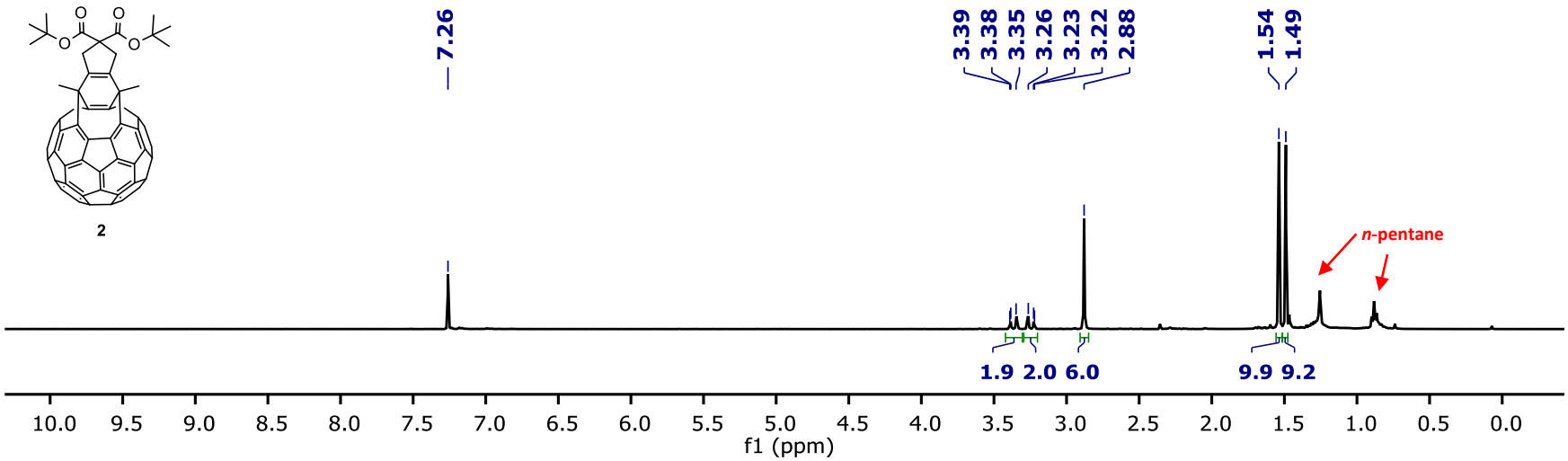

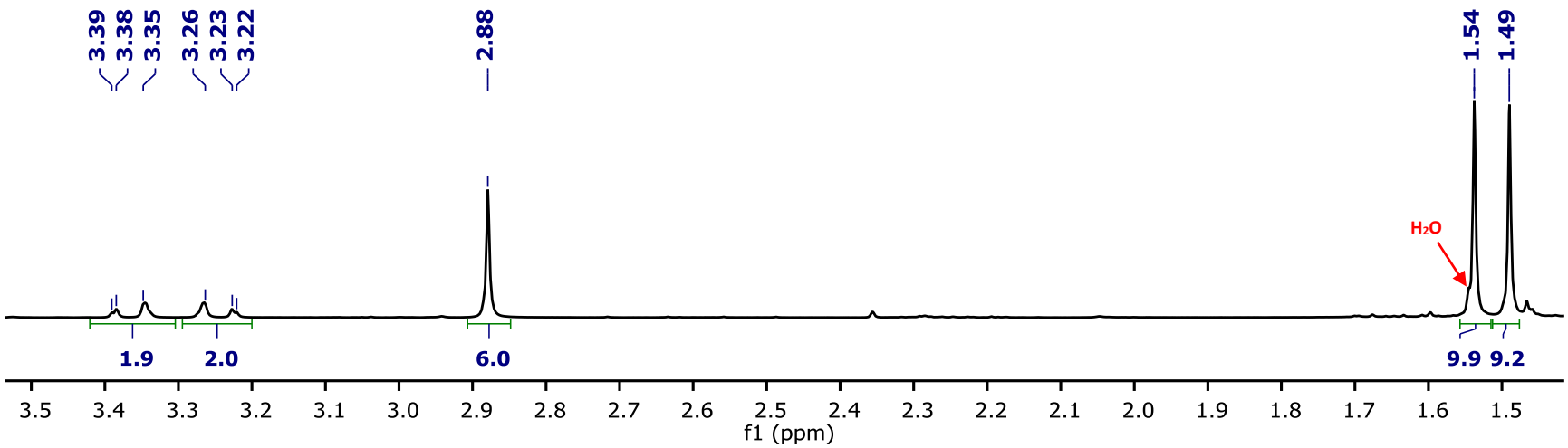

^{13}C NMR (101 MHz, $CDCl_3$)

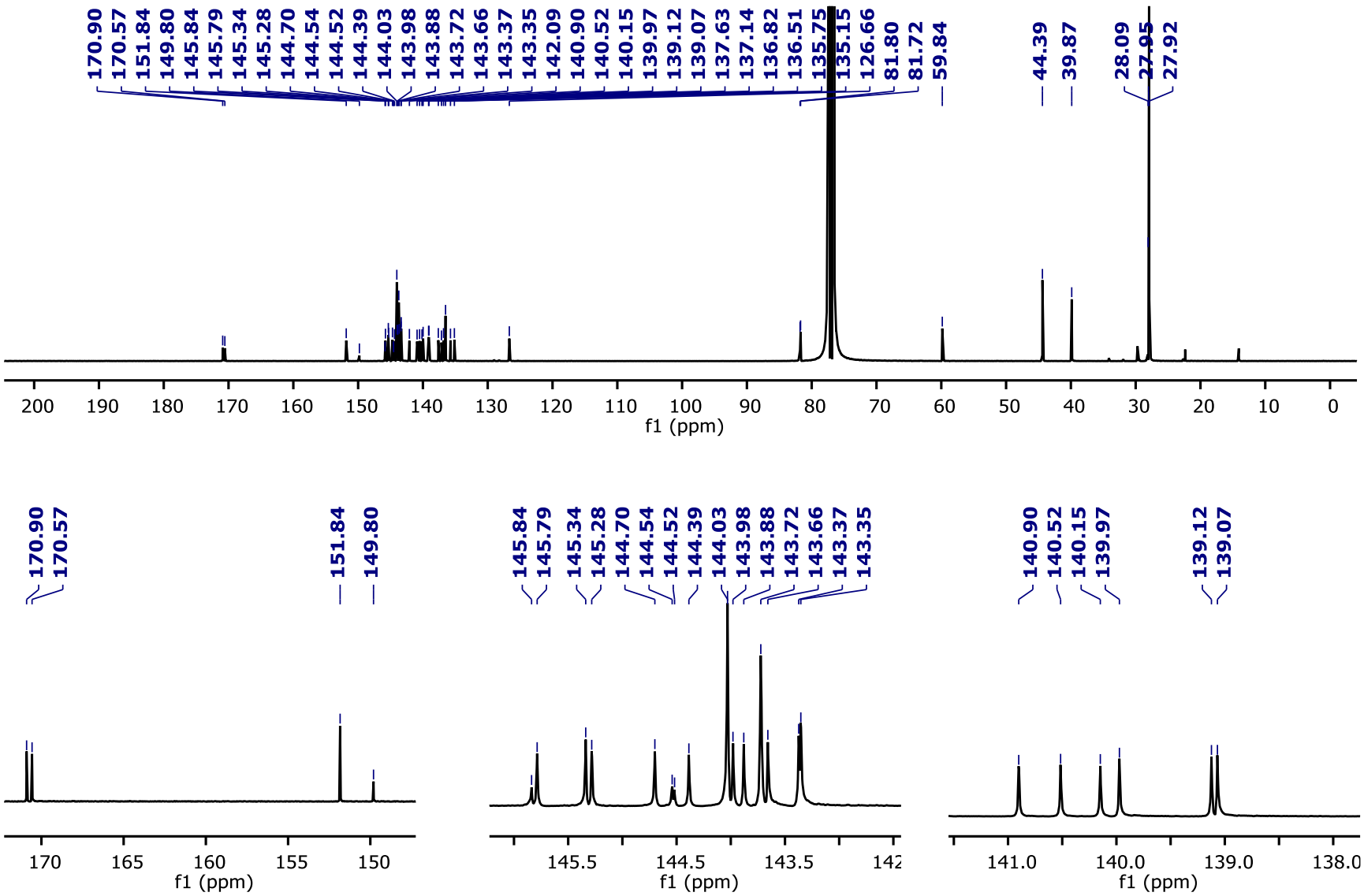

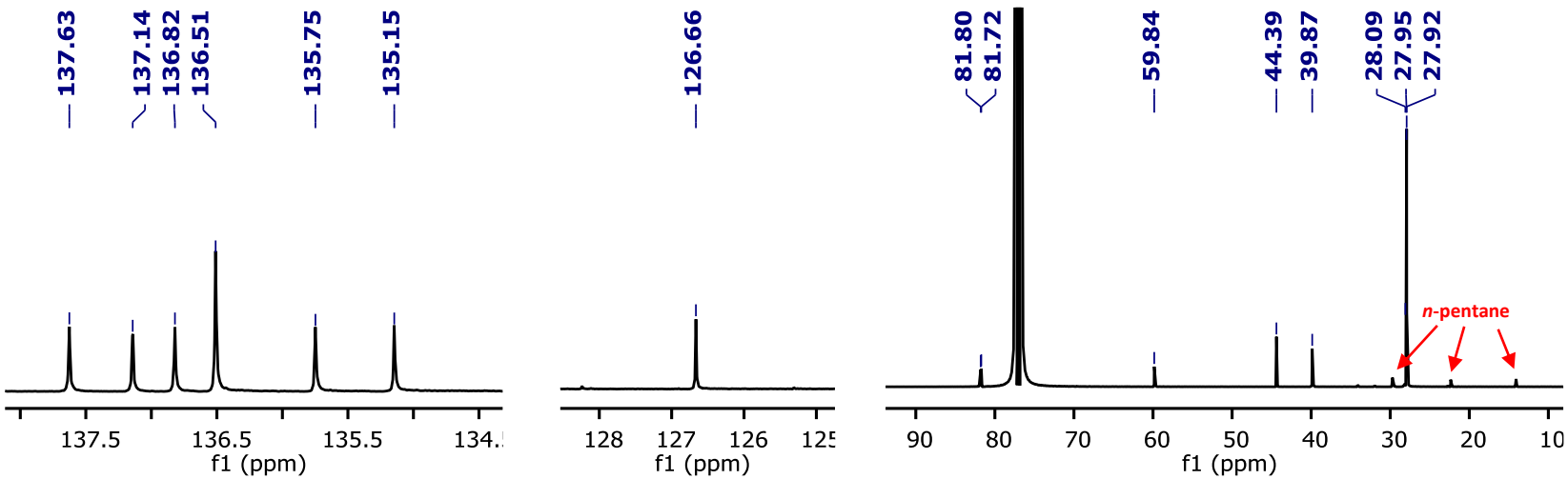
137.63
137.14
136.82
136.51
135.75
135.15
137.5
136.5
135.5
f1 (ppm)
126.66
128
127
126
f1 (ppm)
81.80
81.72
59.84
44.39
39.87
28.09
27.95
27.92
n-pentane
90
80
70
60
50
40
30
20
10
f1 (ppm)

ESI-MS

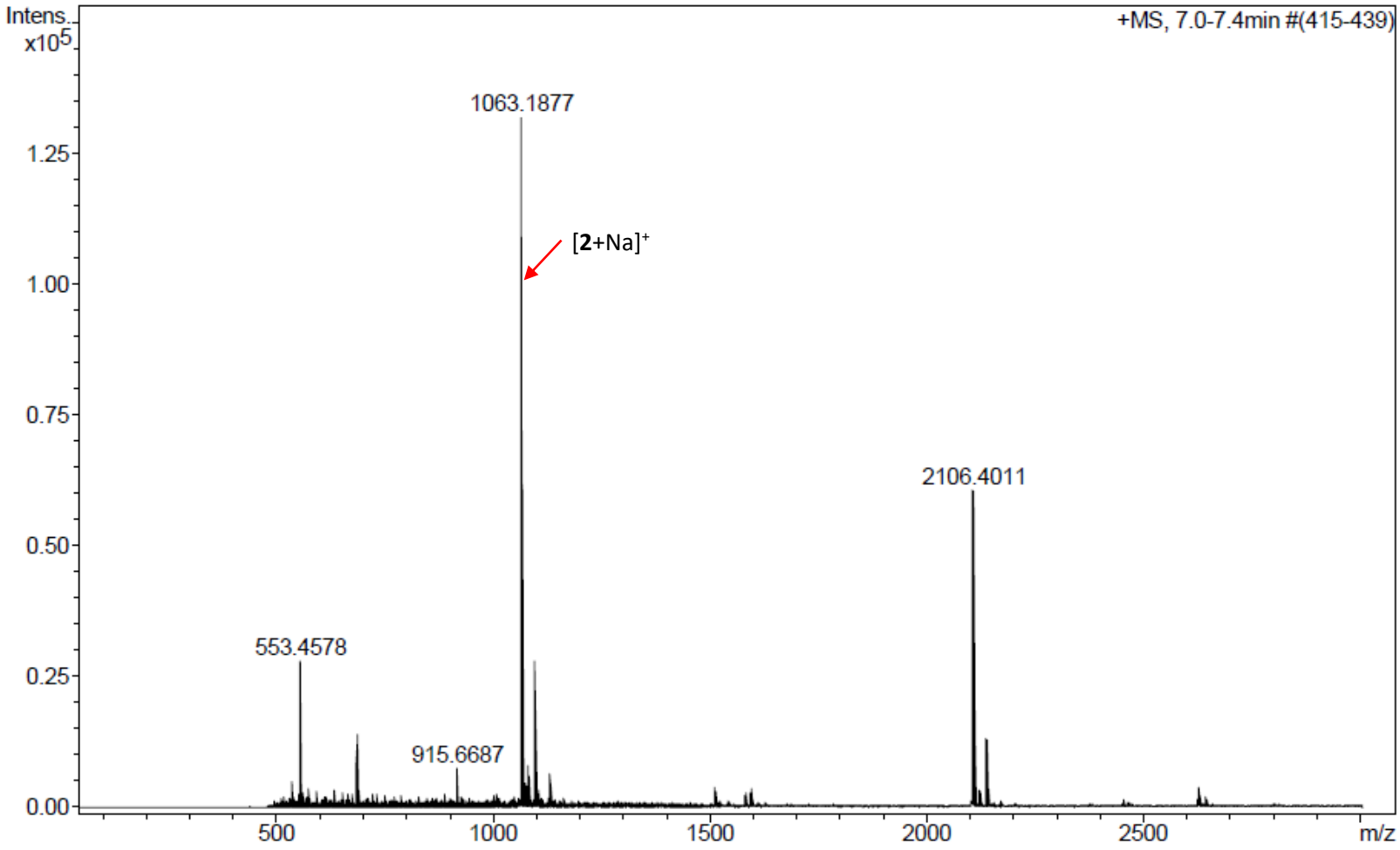
Intens.
x10^5
+MS, 7.0-7.4min #(415-439)
1063.1877
[2+Na]+
2106.4011
553.4578
915.6687
1.25
1.00
0.75
0.50
0.25
0.00
500
1000
1500
2000
2500
m/z

Compound 3

^{1}H NMR (400 MHz, $CDCl_3$)

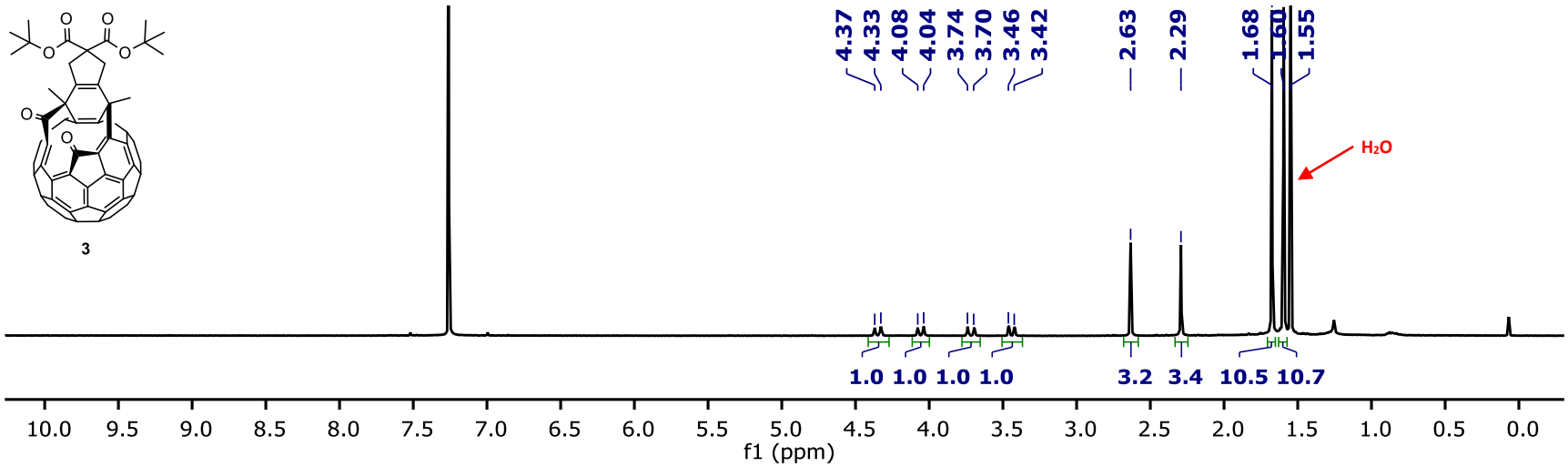

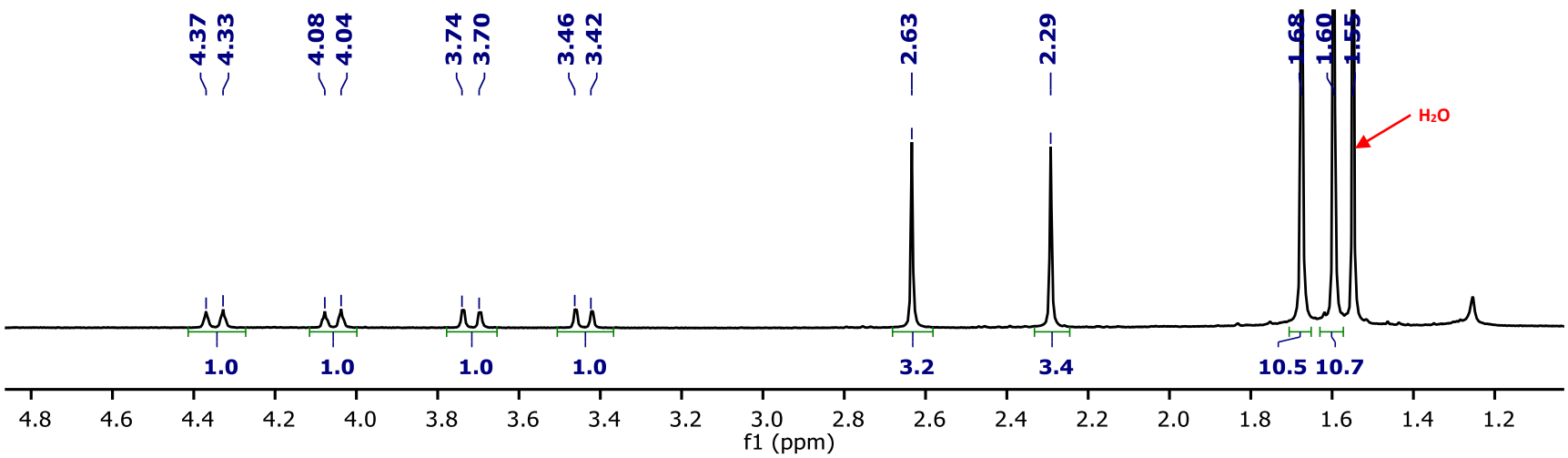

^{13}C NMR (101 MHz, $CDCl_3$)

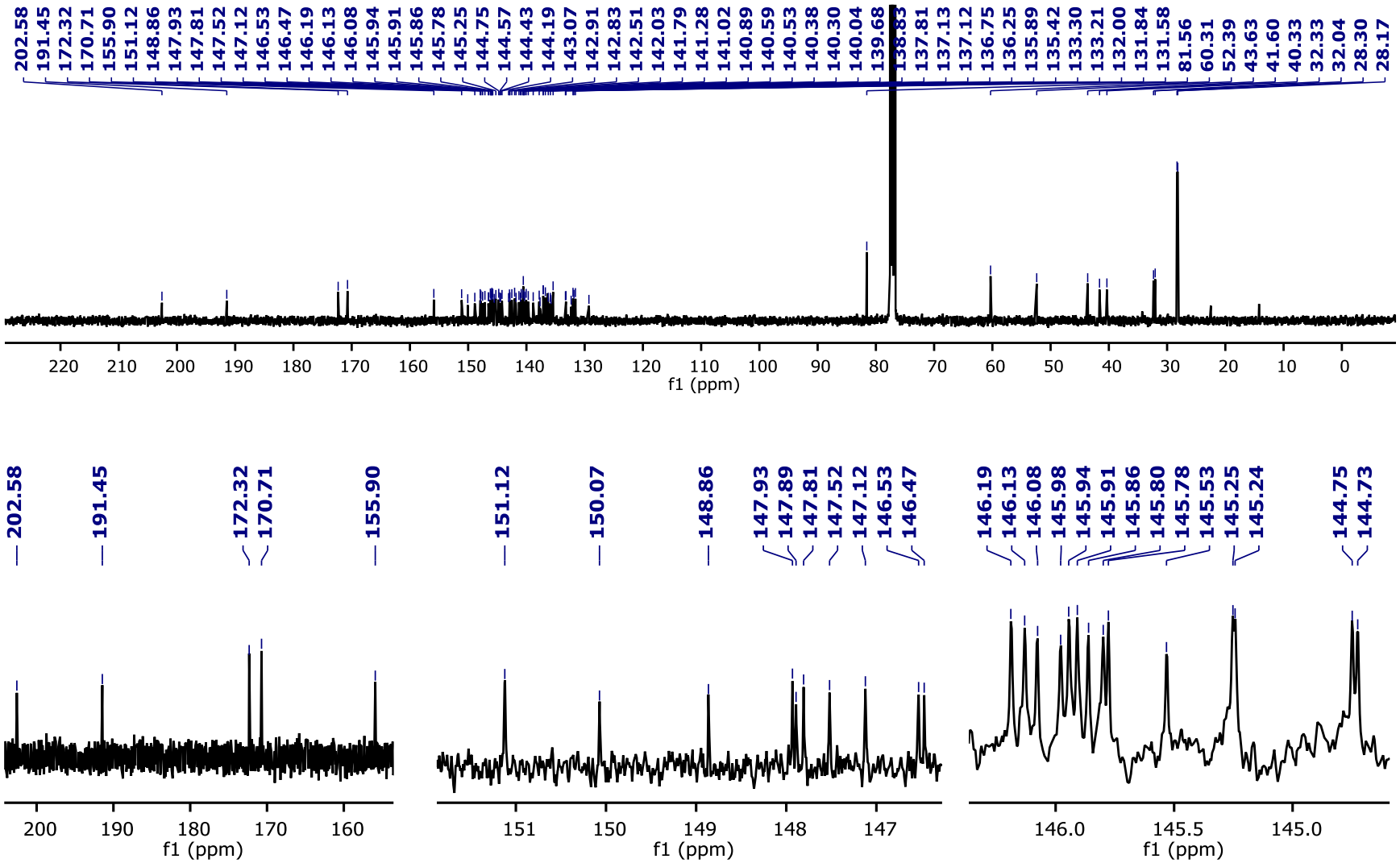

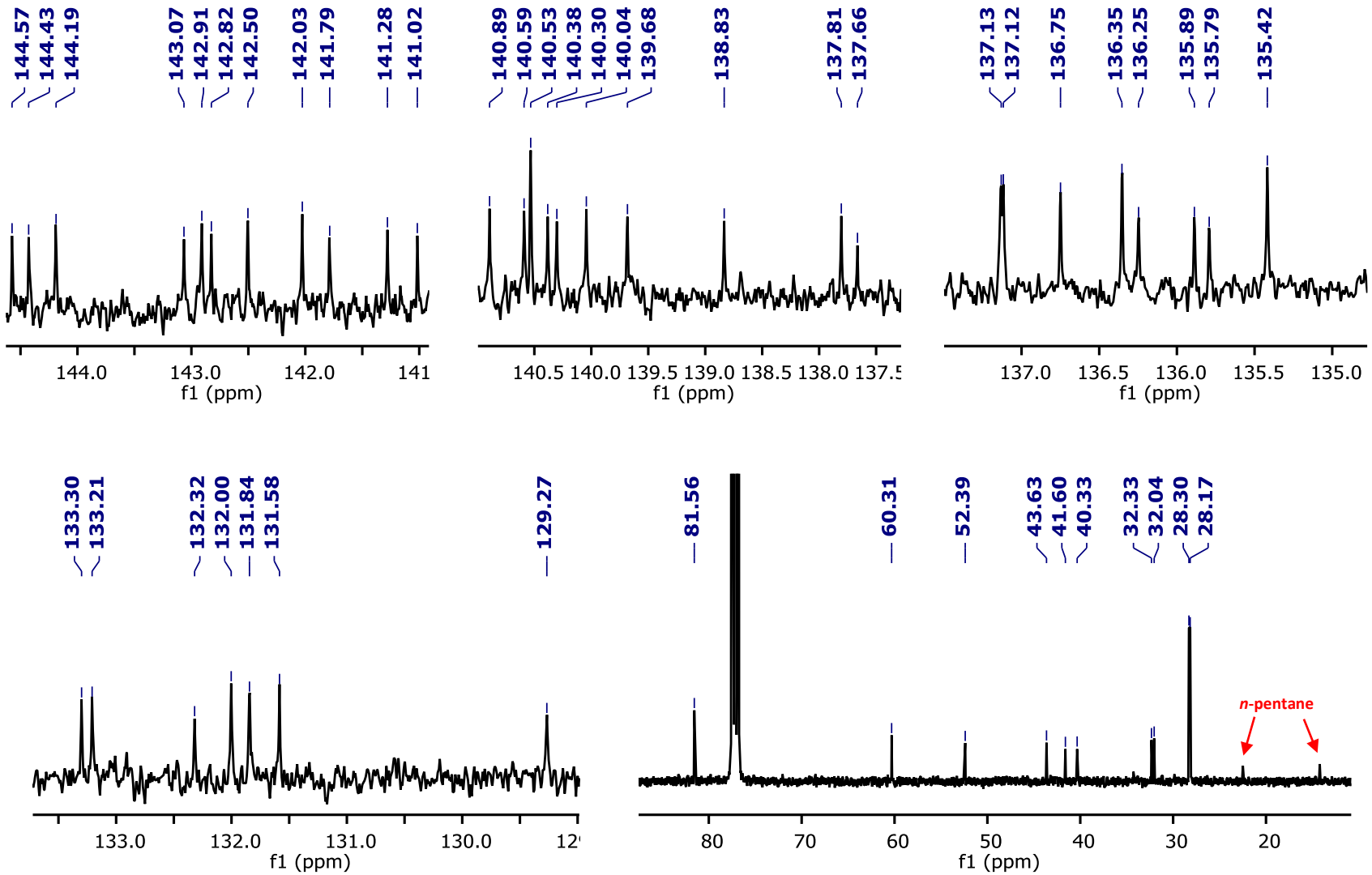
144.57
144.43
144.19
143.07
142.91
142.82
142.50
142.03
141.79
141.28
141.02
144.0
143.0
142.0
141
f1 (ppm)
140.89
140.59
140.53
140.38
140.30
140.04
139.68
138.83
137.81
137.66
140.5 140.0 139.5 139.0 138.5 138.0 137.5
f1 (ppm)
137.13
137.12
136.75
136.35
136.25
135.89
135.79
135.42
137.0
136.5
136.0
135.5
135.0
f1 (ppm)
133.30
133.21
132.32
132.00
131.84
131.58
129.27
133.0
132.0
131.0
130.0
f1 (ppm)
81.56
60.31
52.39
43.63
41.60
40.33
32.33
32.04
28.30
28.17
n-pentane
80
70
60
50
40
30
20
f1 (ppm)

2D NMR COSY ($CDCl_3$)

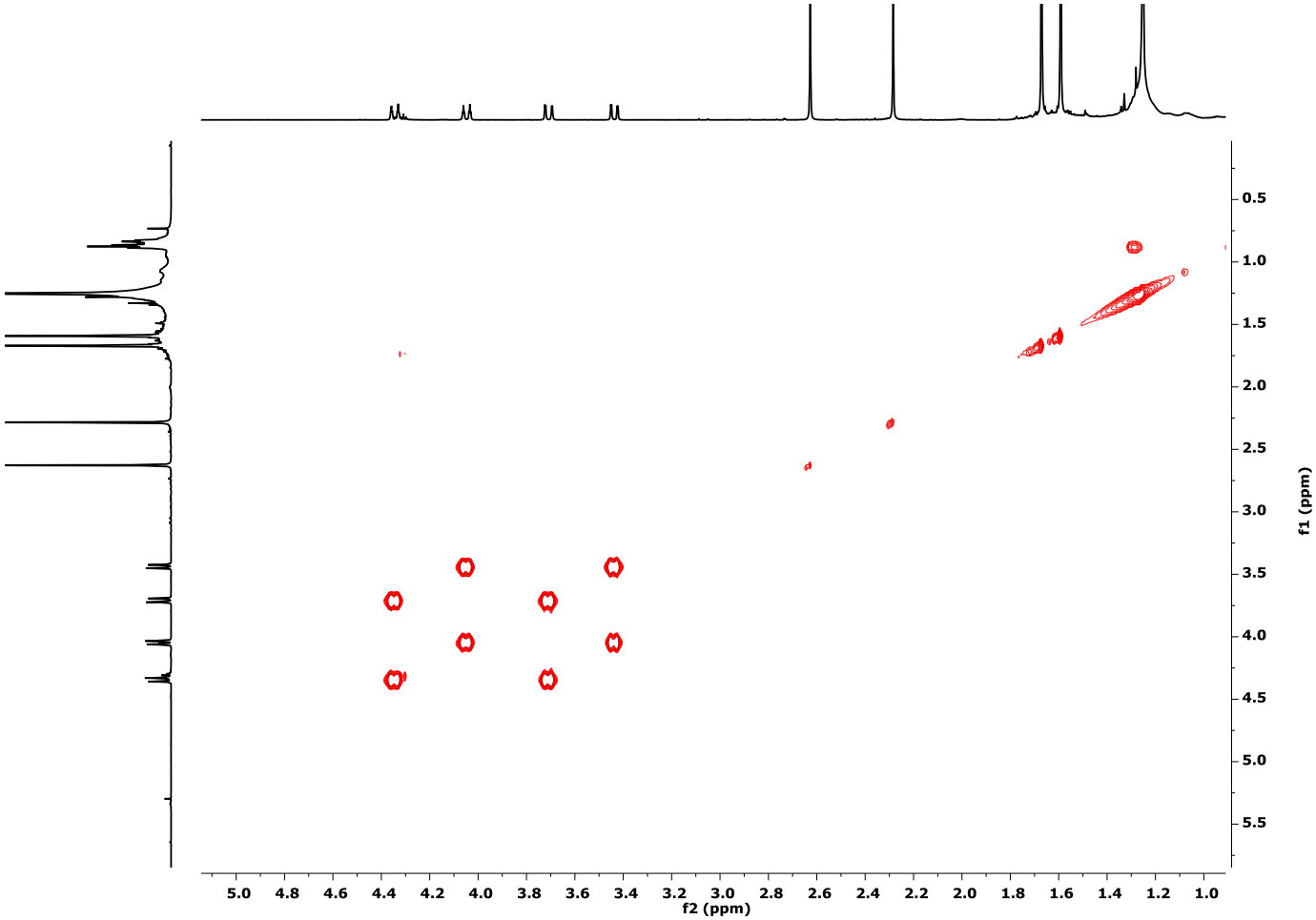

2D NMR HSQC ($CDCl_3$)

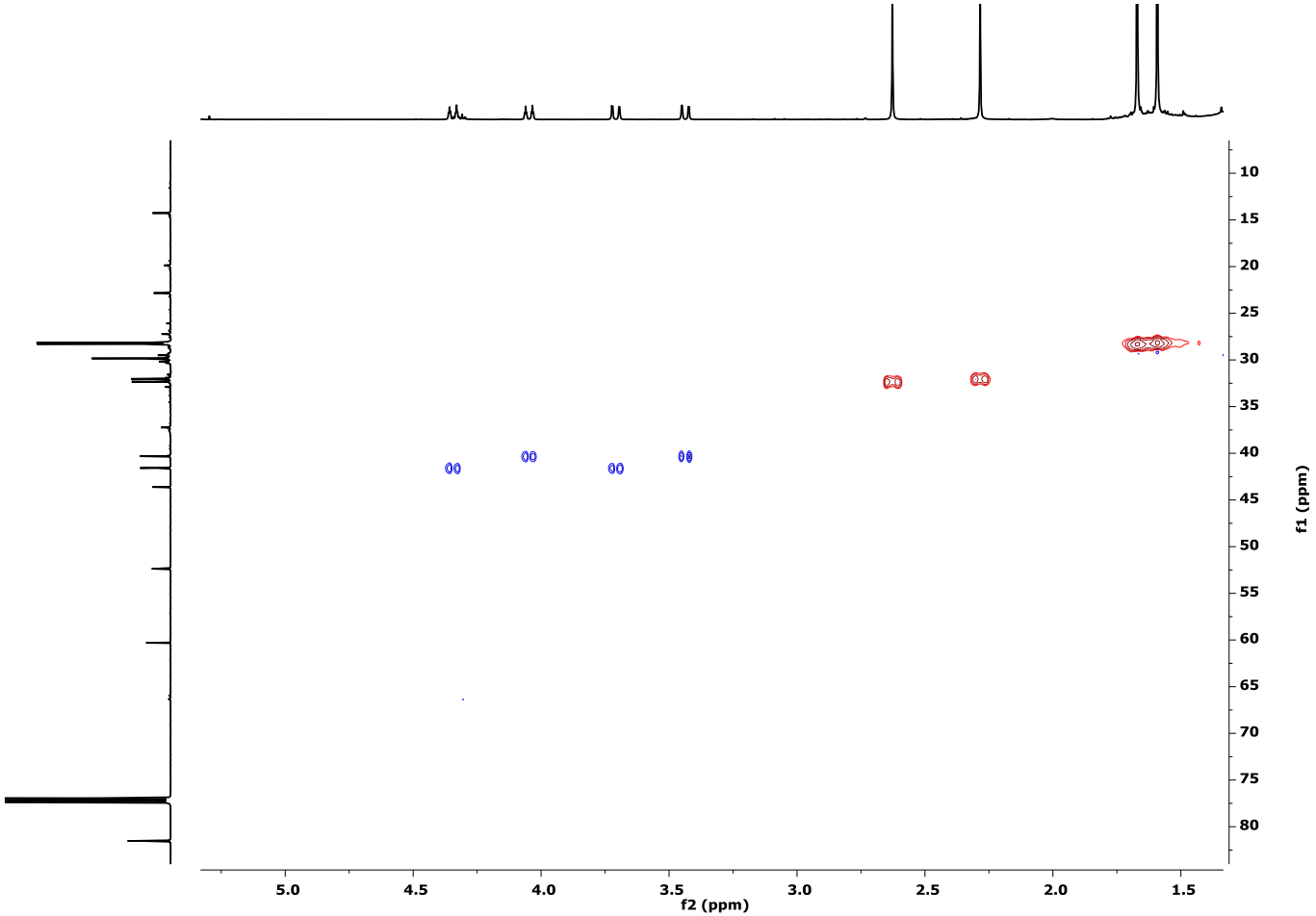

2D NMR HMBC ($CDCl_3$)

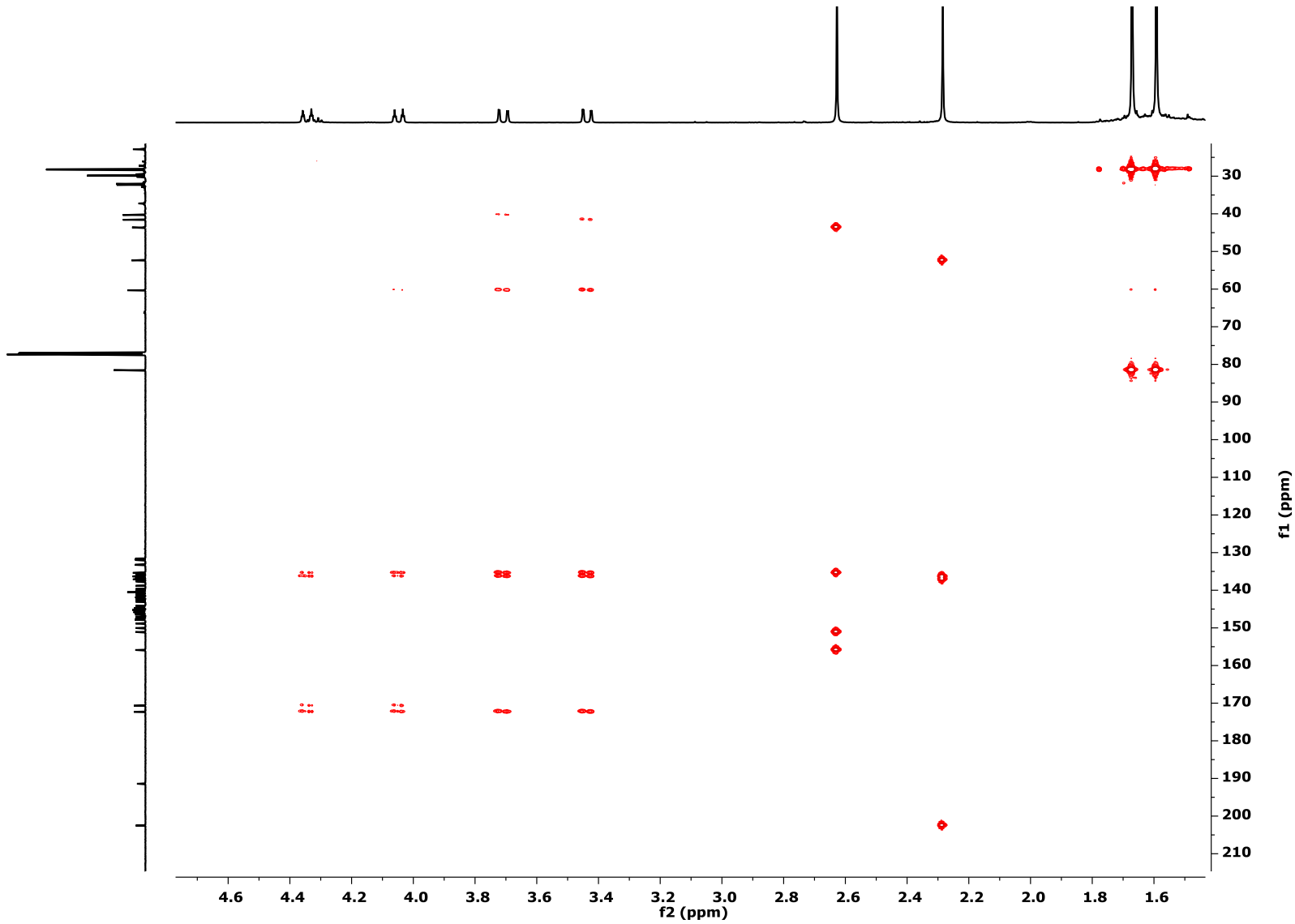

ESI-MS

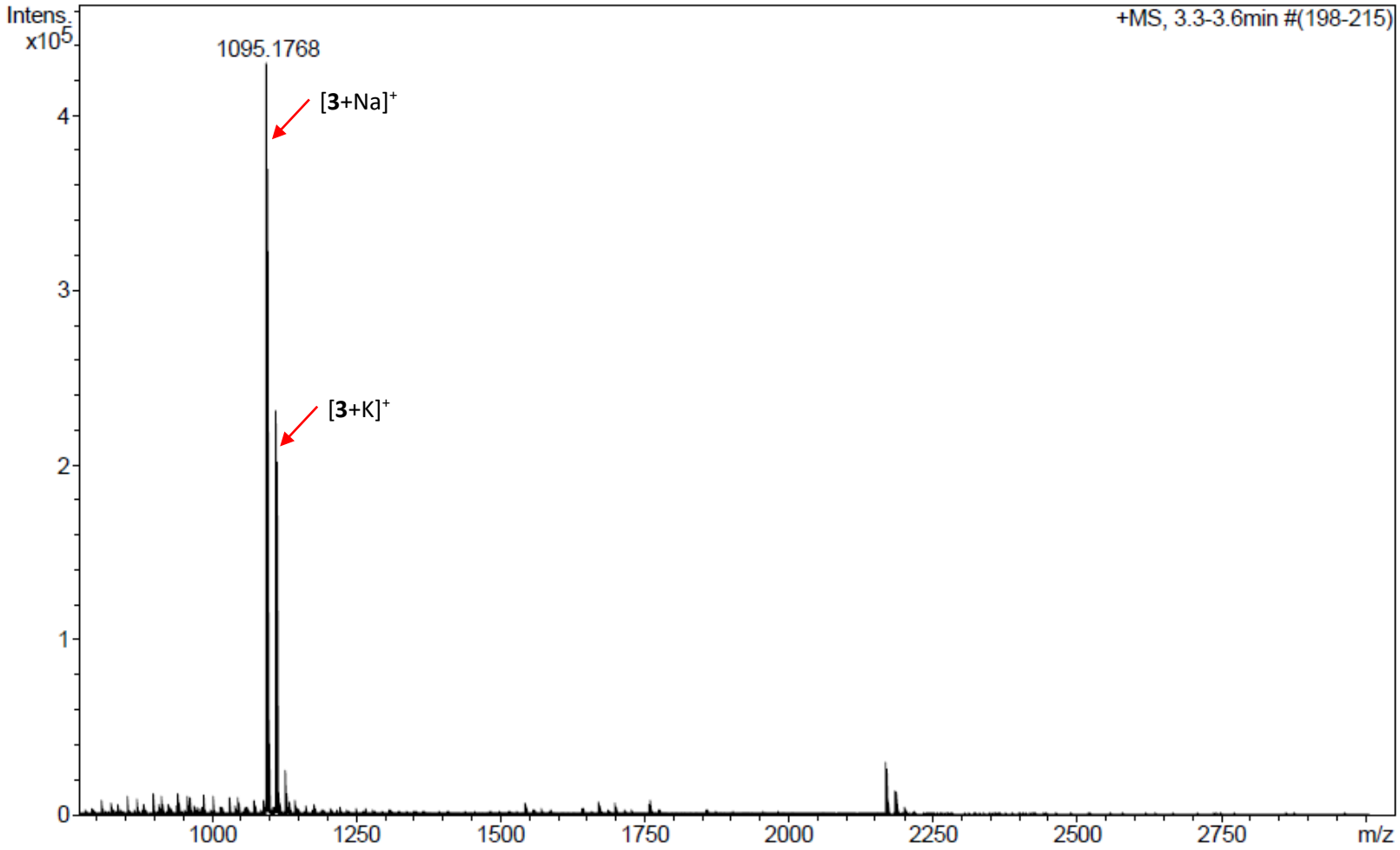
Intens.
x10^5
+MS, 3.3-3.6min #(198-215)
1095.1768
[3+Na]+
[3+K]+
4
3
2
1
0
1000
1250
1500
1750
2000
2250
2500
2750
m/z

References

1 S. Aroua, WB. Schweizer and Y. Yamakoshi, *Org. Lett.* 2014, **16**, 688-1691.

2 C. Sperger, LH.S. Strand and A. Fiksdahl, *Tetrahedron*, 2010, **66**, 7749-7754.

3 A. Artigas, A. Pla-Quintana, A. Lledó, A. Roglans and M. Solà, *Chem. Eur. J.* 2018, **24**, 10653-10661.

4 E. Castro, A. Artigas, A. Pla-Quintana, A. Roglans, F. Liu, F. Perez, A. Lledó, X.-Y. Zhu and L. Echegoyen, *Materials*, 2019, **12**, 1314-1323.

5 Y.N. Yamakoshi, T. Yagami, K. Fukuhara, S. Sueyoshi, and N. Miyata, *J. Chem. Soc., Chem. Commun.* 1994, 517-518.

6 T. Yanai, D. P. Tew and N. C. Handy, *Chem. Phys. Lett.* 2004, **393**, 51-57.

7 F. Weigend and R. Ahlrichs, *Phys. Chem. Chem. Phys.* 2005, **7**, 3297-3305.

8 F. Weigend, *Phys. Chem. Chem. Phys*. 2006, **8**, 1057-1065.

9 S. Grimme, J. Antony, S. Ehrlich and H. Krieg, *J. Chem. Phys.* 2010, **132**, 154104.

10 S. Grimme, S. Ehrlich and L. Goerigk, *J. Comput. Chem.* 2011, **32**, 1456-1465.

11 S. Hirata and M. Head-Gordon, *Chem. Phys. Lett.* 1999, **314**, 291-299.

12 Gaussian 16, Revision A.03, M. J. Frisch, G. W. Trucks, H. B. Schlegel, G. E. Scuseria, M. A. Robb, J. R. Cheeseman, G. Scalmani, V. Barone, G. A. Petersson, H. Nakatsuji, X. Li, M. Caricato, A. V. Marenich, J. Bloino, B. G. Janesko, R. Gomperts, B. Mennucci, H. P. Hratchian, J. V. Ortiz, A. F. Izmaylov, J. L. Sonnenberg, D. Williams-Young, F. Ding, F. Lipparini, F. Egidi, J. Goings, B. Peng, A. Petrone, T. Henderson, D. Ranasinghe, V. G. Zakrzewski, J. Gao, N. Rega, G. Zheng, W. Liang, M. Hada, M. Ehara, K. Toyota, R. Fukuda, J. Hasegawa, M. Ishida, T. Nakajima, Y. Honda, O. Kitao, H. Nakai, T. Vreven, K. Throssell, J. A. Montgomery, Jr., J. E. Peralta, F. Ogliaro, M. J. Bearpark, J. J. Heyd, E. N. Brothers, K. N. Kudin, V. N. Staroverov, T. A. Keith, R. Kobayashi, J. Normand, K. Raghavachari, A. P. Rendell, J. C. Burant, S. S. Iyengar, J. Tomasi, M. Cossi, J. M. Millam, M. Klene, C. Adamo, R. Cammi, J. W. Ochterski, R. L. Martin, K. Morokuma, O. Farkas, J. B. Foresman, and D. J. Fox, Gaussian, Inc., Wallingford CT, 2016.

13 ORCA - an ab initio density functional, and semiempirical program package, version 5.0.3.

14 Neese, F., Software update: The ORCA program system—Version 5.0. *Wiley Interdiscip. Rev. Comput. Mol. Sci.* **2022,** *12* (5), e1606.

15 G. A. Zhurko, Chemcraft 1.80 (build 523b) - graphical program for visualization of quantum chemistry computations. (https://chemcraftprog.com).

16 F. Plasser and H. Lischka, *J. Chem. Theory Comput.* 2012, **8**, 2777-2789.

17 F. Plasser, S. A. Bäppler, M. Wormit and A. Dreuw, *J. Chem. Phys.* 2014, **141**, 024107.

18 A. V.Luzanov and O.A. Zhikol, *Int. J. Quantum Chem.* 2010, **110**, 902-924.

19 A. Klamt and G. Schüürmann, *J. Chem. Soc. Perkin Trans.* 1993, **2**, 799–805.

20 J. Tomasi, B. Mennucci and R. Cammi, *Chem. Rev.* 2005, **105**, 2999-3093.

21 A.A. Voityuk and S.F. Vyboishchikov, *Phys. Chem. Chem. Phys.* 2019, **21***,* 18706-18713.

22 S.F. Vyboishchikov and A.A. Voityuk, *Phys. Chem. Chem. Phys.* 2020, **22***,* 14591-14598.

23 A. Klamt and G. Schüürmann, *J. Chem. Soc. Perkin Trans.* 1993, **2**, 799–805.

24 J. L. Pascual-Ahuir, E. Silla, and I. Tuñón, *J. Comp. Chem.* 1994, **15**, 1127–1138.

25 A. Klamt, *J. Phys. Chem.* 1996, **100**, 3349-3353.

26 R. A. Marcus and N. Sutin, *Biochim. Biophys. Acta, Rev. Bioenerg.* 1985, **811**, 265-322.